



Norwegian University of
Science and Technology

Analysis of Intermediate Band Solar Cell Performance

Eirik Timo Bøe Vilpponen

Master of Science in Physics and Mathematics

Submission date: July 2011

Supervisor: Turid Worren Reenaas, IFY

Analysis of Intermediate Band Solar Cell Performance

Eirik Timo Bøe Vilpponen

July 4, 2011

Abstract

This is the Master's Thesis of Eirik Timo Bøe Vilpponen, and was written at the Department of Physics at the Norwegian University of Science and Technology (NTNU). The thesis is twofold, the first part being the completion of a project undertaken during the fall of 2010. The project concerned the setup of a solar cell current-voltage characterization lab [4] at the same Dept. of Physics.

The second part is an analysis of the current-voltage characteristics of NTNU-made quantum-dot intermediate band solar cells. A strong focus is put on exploring the possibility of utilizing the Two-Diode Model as a means of analysis. The two-diode model has been found to have a good potential for this use, but that it requires a specially made curve fitting computer program to fulfill this potential.

Preface

Handing in this thesis marks the beginning of the end of a fantastic part of my life, and as such it is a bittersweet event. I am extremely grateful for every year I have been given at NTNU and in Trondheim, and will remember this time for the rest of my life. I would like to thank my supervisor, Turid Worren Reenaas, for her assistance over the past academic year, and for inviting me to take part in weekly meetings with her colleagues. These meetings gave me an insight into the academic world of research that I had not seen before. I would like to thank my stepfather, John Buss, for proof reading and giving feedback during the last days of my thesis work. Last, but not least, I would like to thank my fellow students Erik Løkken Walter and Nikolai Hydle Rivedal for seeing me through the last few nerve wrecking hours before my thesis deadline.

Contents

Abstract	iii
Preface	v
1 Introduction	1
1.1 Aim of Thesis	2
2 Theory	3
2.1 A short Introduction to Semiconductors	3
2.2 The pn-Junction	4
2.2.1 Mathematical Analysis of the PN-Junction	7
2.3 Intermediate Band Solar Cells	13
2.4 Diode Models	16
2.4.1 The Interpretation of D_1 and D_2	16
3 Continuation of Project Work	19
3.1 Instructions of Use	22
3.1.1 The Solar Simulator	22
3.1.2 Sourcemeter and Computer	22
3.1.3 The Thermo-Box	26
3.2 Verification of Laboratory Setup	26
4 Simulations	31
4.1 The parameters of the two-diode model	31
4.1.1 The Ideal Case	33
4.1.2 Parasitic Resistances	33
4.1.3 Increased Current	34
4.1.4 Temperature Effects	34
4.1.5 Ideality factors	35
4.1.6 The Saturation Currents	35

5	Results	41
5.1	Measurements	41
5.2	Curve Fitting	41
6	Discussion	47
7	Conclusions and Further Work	49
A	Current-Voltage characteristics for all cells	53
B	Output file	59

List of Figures

2.1	Typical band structure of pure silicon	4
2.2	p-type and n-type material before contact.	5
2.3	The pn-junction in equilibrium	6
2.4	Illustration of band bending at a PN-junction	7
2.5	Common types of recombination	8
2.6	Illustration of a pn-junction	11
2.7	IV-Characteristics	14
2.8	Illustration of the energy levels in an IBSC	15
2.9	The one diode model.	17
2.10	The two diode model.	18
2.11	Different ideality factors for different materials and bias voltages.	18
3.1	The laboratory setup.	20
3.2	The Solar Simulator Front Panel.	21
3.3	Calibration of the Solar Simulator.	23
3.4	Sourcemeeter Front.	24
3.5	Frontpanel of LabVIEW VI.	25
3.6	Different measurements made on cell As 564.	27
3.7	Different measurements made on cell As 566.	28
3.8	Different measurements made on cell As 568.	28
3.9	Different measurements made on cell As 578.	29
3.10	Laboratory Precision	29
4.1	The two-diode model in OrCAD/pSpice.	32
4.2	The output of the ideal one-diode model.	33
4.3	Output of the two-diode model with changing series resistance.	34
4.4	Output of the two-diode model with a varying shunt resistance.	35
4.5	The effect of both a high series- and a low shunt resistance on the IV-curve.	36
4.6	Two-diode model output with increasing current	37
4.7	The effect of temperature on the two-diode model output	38
4.8	The effect of n_1 on the one-diode model	38

4.9	The gained degree of freedom by the addition of a second diode to the one-diode model.	39
4.10	The effect of j_{02} on the two-diode model.	39
5.1	IV-characteristics for cell As 567.	43
5.2	Current-voltage characteristics of all cells.	44
5.3	An attempt at curve fitting.	45
A.1	Current-voltage characteristics for cell no. As 564.	53
A.2	Current-voltage characteristics for cell no. As 566.	54
A.3	Current-voltage characteristics for cell no. As 567	54
A.4	Current-voltage characteristics for cell no. As 568	55
A.5	Current-voltage characteristics for cell no. As 569.	55
A.6	Current-voltage characteristics for cell no. As 570.	56
A.7	Current-voltage characteristics for cell no. As 578	56
A.8	Current-voltage characteristics for cell no. As 579.	57

Chapter 1

Introduction

There is little doubt that the carbon based energy of the 19th and 20th century soon must be replaced by some other means of energy production. There are many competing technologies and among many alternatives solar energy presents a real possibility. Both private energy companies and entire governments share an interest in the application and research of solar power. As the world population increases and the standard of living in the third world rises, it has become even more crucial to meet demands for clean and cost-effective energy.

The first and foremost strength of solar power is clearly the abundance of free energy available. The earth receives approximately 174 petawatts [1] of power from the sun and it has always been our most important energy source. Being able to harness this energy in an efficient way would provide a virtually inexhaustible supply of power that would aid the entire human race.

When exposed to sunlight, photovoltaic devices based on semiconductors supply directly usable electric power. As opposed to the low-tech thermal solar energy, photovoltaics require little upkeep or maintenance after their initial setup. They may also be used in small units independent of both the electric grid and large scale power plants.

The two major drawbacks of solar cells are low efficiency and high cost. Solar panels are notoriously ineffective at transforming sunlight into power and a typical efficiency would be around 15 % [2]. It is only the very high amount of available raw energy (the sunlight) that allows it to compete. While the silicon used in most kinds of solar cells is abundant on earth, the effort required to refine it to the needed purity is large. This makes them expensive to produce and causes the initial investment price to be relatively high. It is with this in mind that research scientists study and try to improve the characteristics of solar cells. It is clear that there still is a long way to go

before they can be used as a major supplier of power. It is also clear that at least one of the problems mentioned above needs to be resolved before this can happen. If success is achieved however, the rewards would be great, as sustainable, clean and easy energy would be readily available.

1.1 Aim of Thesis

There are three aims of this thesis. The first is to continue and complete a project started the fall of 2010 concerning the setup of a solar cell characterization laboratory. This includes updating the lab and testing its capabilities. Secondly, the current-voltage characteristics and efficiencies of eight NTNU-made intermediate band solar cells will be examined. Thirdly, an analysis will be made of the two-diode model and its potential in solar cell research.

Chapter 2

Theory

2.1 A short Introduction to Semiconductors

A semiconductor is a solid material that can act as both an electrical insulator or conductor depending on external and internal parameters. Temperature is an example of one such parameter and the addition of impurities to the material is another. Adding impurities that add negative or positive charge carriers are of great interest as it permanently changes the material in a controllable fashion. Introducing atoms with more valence electrons than the base element results in the material being n-doped, it has an excess of negative charge carriers (electrons). Introducing atoms with fewer valence electrons gives a p-doped material, it will have an excess of positively charged charge carriers (holes). Examples of this are silicon doped with phosphorous (n-type) and silicon doped with boron (p-type). It is well known (The reader is referred to any book on solid-state physics) that electrons within the semiconductor material are unable to occupy certain energy states, but is forced to move (energetically) in energy bands. The common starting point for semiconductors is shown in fig. 2.1. This figure shows a 'valence band' and a 'conduction band' separated by a 'band gap'. The figure also shows what is known as the 'fermi level'. The fermi level is defined to be the energy level of the most energetic occupied electron state within the system at $T = 0$ K. As temperature rises, electrons are able to occupy energy states higher than the fermi level, by means of thermal excitations. Electrons in the valence band are moving in the atomic orbitals of the parent atoms, electrons in the conduction band are unlocalized and do not belong to any one atom. As such they are free to move around in the crystal. Physically, a hole is actually the absence of an electron in the valence band. Since it can be advantageous to think of it as a real particle, this has become the norm. The addition of

these "dopants" changes the fermi level of the crystal. n-doping the material causes the fermi level to rise while p-doping causes it to lower when compared to the undoped, intrinsic case. See fig (2.2) for an illustration. The reader is referred to books on semiconductor physics such as *The Physics of Solar Cells* by Jenny Nelson [3] for a more thorough explanation if it is needed.

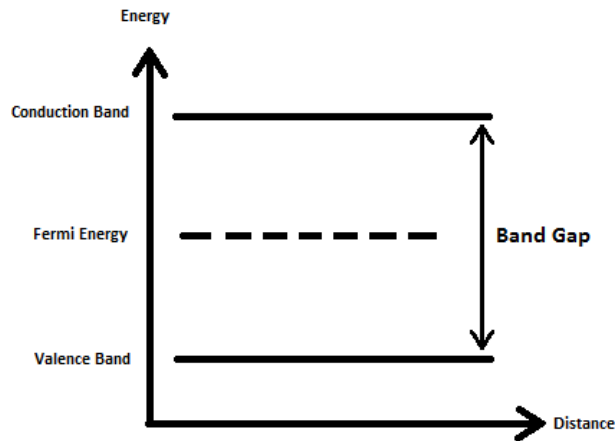


Figure 2.1: Typical band structure of pure silicon

2.2 The pn-Junction

The standard diode is one of the most basic electronic devices one can construct from semiconductors. See fig. 2.3. It consists of a piece of p-type semiconductor material in physical contact with a similar piece of n-type material. When the two semiconductor pieces are put together, the difference in fermi levels will cause the charge carriers to redistribute themselves throughout the system. Equilibrium occurs when the fermi level is flat throughout the material. The redistribution affects the volume close to the pn-interface which is called the "Space Charge Region" (SCR) or Depletion Region. Electrons from the n-side flow into the p-material where they recombine with the holes present there. This recombination has two important consequences. Firstly; the space charge region runs out of free charge carriers. Secondly; the areas on either side of the interface become electrically charged with the addition of an electron or a hole. It is important to keep in mind that as opposed to the electrons who are free to roam the crystal structure of the silicon, the charged atoms are tied down in their respective positions. This results in a static electric field pointing through the depletion region from the n-side to the p-side, giving rise to an electric potential difference over

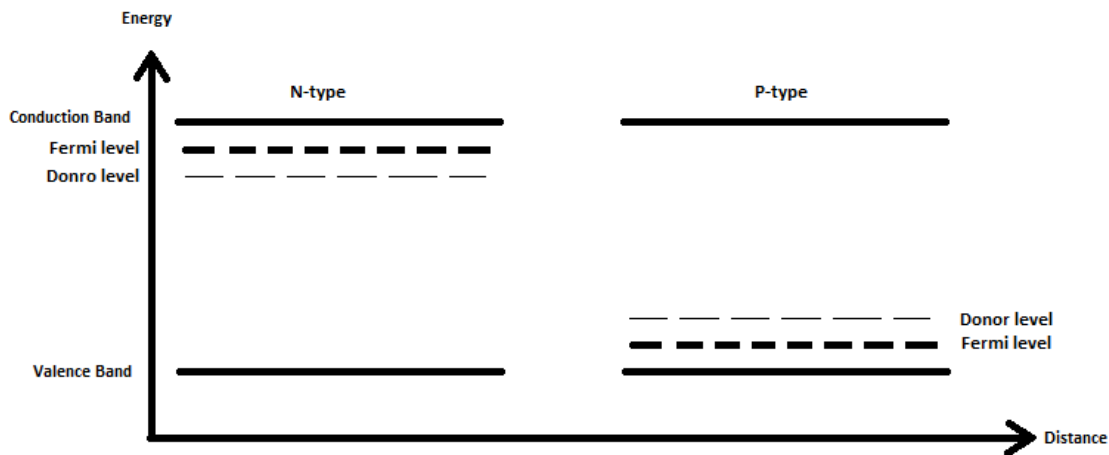


Figure 2.2: p-type and n-type material before contact.

the space charge region. See the bottom two graphs of fig. 2.3. This electric potential will cause so called "band bending" and as a result the potential of the conduction band on the p-side will be higher than on the n-side. See fig. 2.4 for an illustration.

There are several uses for the simple diode and in this text the focus will be on its use as a solar cell. If a diode has the correct shape and is illuminated by electromagnetic radiation (sunlight), it is able to produce electrical power. It does this by means of the photovoltaic effect. When light shines on the pn-junction the photons will excite electrons in the material and break the covalent bonds that bind them to their parent atom. This event is often called "creating an electron/hole pair". Whenever this happens in the depletion region, the electron will be forced into the n-material by the electric field. This causes a build-up of charge able to do useful work. The light has the same effect in the neutral p- and n-regions, but as there is no electric field to separate the charges there, they quickly recombine without contributing to useful work. There are several ways an electron and hole can recombine and the three most common kinds of recombination are radiative recombination, Auger recombination and Shockley-Read-Hall recombination. See fig 2.5.

Radiative recombination occurs when an electron in the conduction band loses energy by emitting electromagnetic radiation and deexcites down to the valence band. It is often thought of as the most basic of the three types. Auger recombination is when an energy rich electron in the conduction band collides with a localized electron in the valence band and loses its energy. There is no emitted radiation during Auger recombination. Shockley-

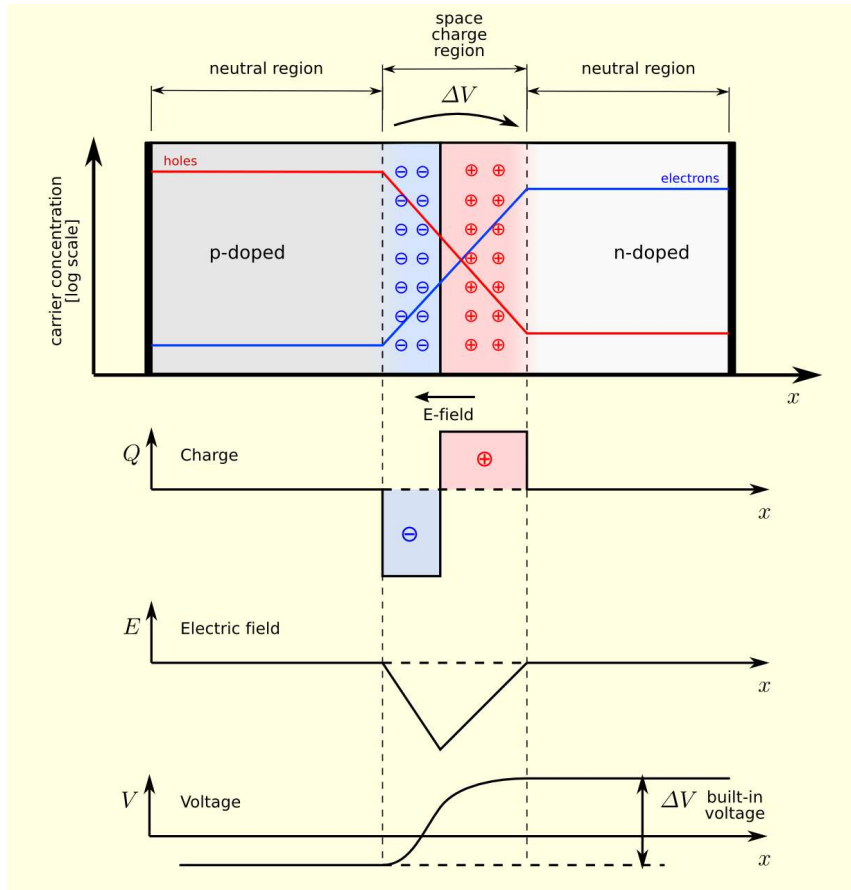


Figure 2.3: The pn-junction in equilibrium. The image is taken from <http://en.wikipedia.org/wiki/File:Pn-junction-equilibrium-graphs.png>. It was downloaded on the 8th of December 2010.

Read-Hall recombination occurs when electrons deexcite through impurity states in the crystal lattice. These states usually occur grouped together in so called "recombination centers". Recombination is radiative and around the recombination centers it can be more intense than the other kinds of recombinations. Both Auger and SRH recombination can be avoided, but radiative recombination is an inherent process in the crystal and cannot be removed. Auger recombination can be reduced by having a low electron injection. In other words, having a relatively low current flowing through the cell. SRH recombination can be avoided by having pure crystals without imperfections. It should be noted that all the recombination methods can act as generation methods if they are run in reverse.

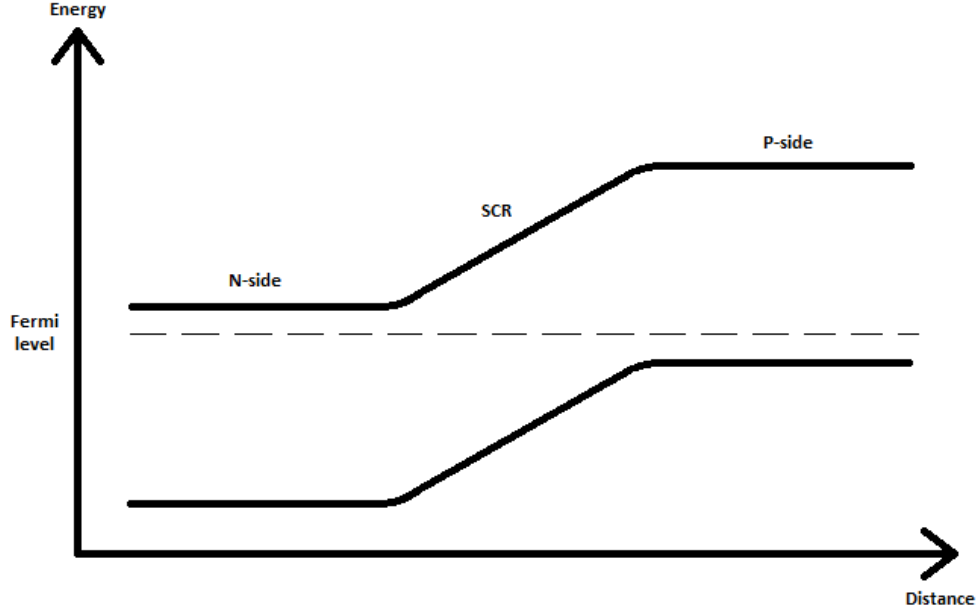


Figure 2.4: Illustration of band bending at a PN-junction. Note the constant fermi level.

2.2.1 Mathematical Analysis of the PN-Junction

It is possible to achieve an analytical function for the current through a diode, but some simplifying assumptions are required. A common starting point is the assumption of charge preservation and Gauss' law applied to an imagined PN-junction as shown in fig. 2.6.

$$\frac{\partial n}{\partial t} = \frac{1}{q} \frac{\partial J_n}{\partial x} + G_n - U_n \quad (2.1)$$

$$\frac{\partial p}{\partial t} = \frac{1}{q} \frac{\partial J_p}{\partial x} + G_p - U_p \quad (2.2)$$

$$\frac{\partial F}{\partial x} = -\frac{\partial^2 \phi}{\partial x^2} = -\frac{q}{\epsilon_s} (n - p - \rho_{fixed}(x)) \quad (2.3)$$

For simplicity the entire analysis is done in one dimension, along the x-axis. Here n and p are the electron and hole densities, F is used for the electric field and J_n and J_p are the electric current densities caused by electrons and holes. One should note that

$$J(x) = J_n(x) + J_p(x) \quad (2.4)$$

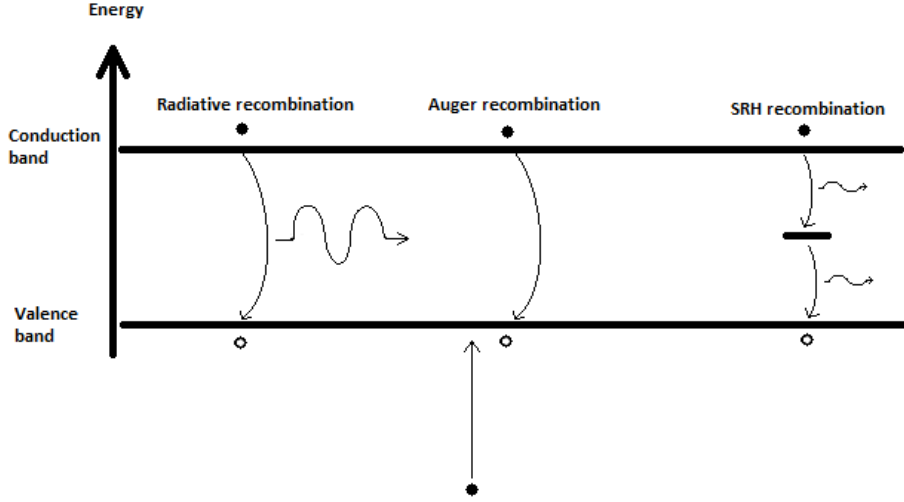


Figure 2.5: The three common kinds of recombination; Radiative-, Auger- and Shockley-Read-Hall recombination.

is the total current-density. G and U are the electron and hole generations and recombinations. ϕ is the electric potential and ρ_{fixed} is the localized charge caused by ionized dopants. Assuming steady-state operation and an unchanging crystal structure and crystal composition:

$$\frac{\partial n}{\partial t} = \frac{\partial p}{\partial t} = 0 \quad (2.5)$$

$$J_n(x) = qD_n \frac{\partial n}{\partial x} + q\mu_n n F \quad (2.6)$$

$$J_p(x) = -qD_p \frac{\partial p}{\partial x} + q\mu_p p F \quad (2.7)$$

Equations (2.6) and (2.7) express how the current density can be split into diffusive and drift currents. n and p are electron and hole densities, μ_n and μ_p are the electron and hole mobilities and D_n and D_p are diffusion coefficients. Note that the assumption of unchanging structure and composition implies that (2.6) and (2.7) are invalid at junctions between different kinds of crystals.

Rearranging and combining expressions (2.1) - (2.7) yields

$$D_n \frac{\partial^2 n}{\partial x^2} + \mu_n F \frac{\partial n}{\partial x} + \mu_n n \frac{\partial F}{\partial x} - U + G = 0, \quad (2.8)$$

$$D_p \frac{\partial^2 p}{\partial x^2} + \mu_p F \frac{\partial p}{\partial x} + \mu_p p \frac{\partial F}{\partial x} - U + G = 0. \quad (2.9)$$

The two key assumptions used to simplify the system are called the depletion approximation and the superposition approximation. The depletion approximation assumes that the depletion region around the pn-interface is completely stripped of its charge carriers. It further assumes that the entire voltage drop of the diode occurs linearly across the depletion region. In the superposition approximation the recombination rate U in the expression above is assumed to be linear in the amount of minority carriers in the region. This approximation is justified if the difference in majority and minority charge carrier densities are large, i.e:

$$n \gg p \quad (2.10)$$

in the n-region, and

$$p \gg n \quad (2.11)$$

in the p-region. The recombination is then assumed to be linearly dependent on the minority carrier density:

$$U_p = \frac{n - n_0}{\tau_n} \quad (2.12)$$

in the p-region, and

$$U_n = \frac{p - p_0}{\tau_p} \quad (2.13)$$

in the n-region. Adapting (2.8) and (2.9) to the three regions of the diode gives three contributions to the total current that can be summed together to give the total diode current. As mentioned before, the depletion approximation assumes that the total voltage drop over the diode occurs entirely across the depletion region. This implies that the voltage stays constant in the neutral p- and n-regions which again implies that the electric field is zero by definition of the electric potential:

$$\mathbf{F} = -\nabla V \quad (2.14)$$

This leaves (2.8) and (2.9) in the following forms:

$$\frac{\partial^2 n}{\partial x^2} - \frac{n - n_0}{L_n^2} + \frac{g(E, x)}{D_n} = 0 \quad (2.15)$$

in the p-type region, and

$$\frac{\partial^2 p}{\partial x^2} - \frac{p - p_0}{L_p^2} + \frac{g(E, x)}{D_p} = 0 \quad (2.16)$$

in the n-type region. Here L_n^2 and L_p^2 are diffusion lengths of electrons and holes given by: $L_n = \sqrt{\tau_n D_n}$ for electrons and similarly for holes. $g(E, x)$ is the pair generation rate at position x . It should be noted that these are the minority charge carrier densities. The majority densities are constant and equal to N_D and N_A . Setting the electrical field \mathbf{F} to zero in equations (2.6) and (2.7) gives the expression for minority charge currents in the neutral p- and n- regions:

$$j_n(E, x) = qD_n \frac{dn}{dx}, \quad \text{p - region} \quad (2.17)$$

$$j_p(E, x) = -qD_p \frac{dp}{dx}, \quad \text{n - region} \quad (2.18)$$

As these equations are functions of both position in the semiconductor material and the energy of the incoming radiation, they may be integrated over the spectrum of radiation to yield functions that only depend on the position:

$$J_n(x) = \int j_n(E, x) dE \quad (2.19)$$

$$J_p(x) = \int j_p(E, x) dE \quad (2.20)$$

The following boundary conditions may be used to solve equations (2.17) and (2.18)

$$n - n_0 = \frac{n_i^2}{N_a} (e^{\frac{qV}{k_B T}} - 1), \quad x = -w_p \quad (2.21)$$

$$p - p_0 = \frac{p_i^2}{N_a} (e^{\frac{qV}{k_B T}} - 1), \quad x = w_n \quad (2.22)$$

$$D_n \frac{dn}{dx} = S_n (n - n_0), \quad x = -x_p \quad (2.23)$$

$$D_p \frac{dp}{dx} = S_p (p - p_0), \quad x = x_n \quad (2.24)$$

Here S_n and S_p from equations (2.23) and (2.24) are surface recombination rates at the outer surfaces of the diode. Boundary conditions (2.21) and (2.22) show the minority carrier density's dependence on external bias. Minority carriers are said to be "injected" into the pn-junction by an external voltage. In a steady state situation charge conservation requires the electron and hole currents to be constant. Setting x to be equal to the depletion widths of the SCR, w_n and w_p , one gets:

$$J_n(x) = J_n(-w_p) \quad (2.25)$$

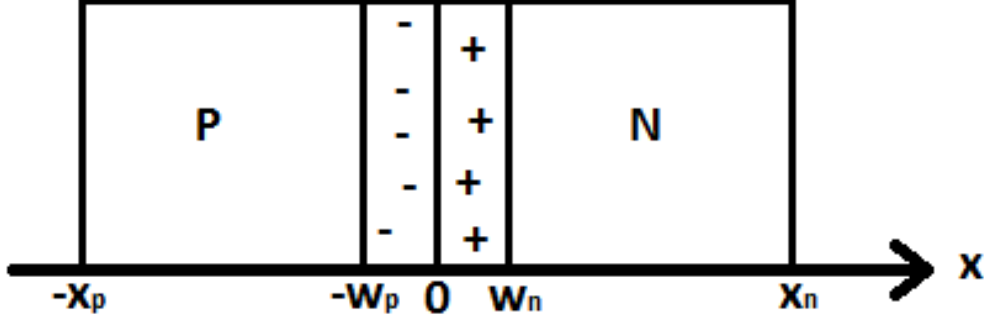


Figure 2.6: Simplification of a diode with the positions w_p , w_n , x_p and x_n marked. The SCR is the area between $-w_p$ and w_n

$$J_p(x) = J_p(w_n) \quad (2.26)$$

The depletion approximation requires the quasi-Fermi energy of the electrons and the holes to be constant across the depletion region:

$$E_{Fn}(x) = E_{Fn}(w_n) \quad (2.27)$$

$$E_{Fp}(x) = E_{Fp}(-w_p) \quad (2.28)$$

$$qV = E_{Fn}(x) - E_{Fp}(x), \quad -w_p < x < w_n \quad (2.29)$$

Assuming a steady-state situation and combining (2.1) and (2.2) gives the expression for the SCR current:

$$J_{SCR} = q \int_{-w_p}^{w_n} (U - G) dx. \quad (2.30)$$

Here, the recombination, U , may be found by analyzing the electron and hole densities using equations (2.27) through (2.29) and the equations

$$n = n_i e^{\frac{E_{Fn} - E_i}{k_B T}} \quad (2.31)$$

and

$$p = n_i e^{\frac{E_i - E_{Fp}}{k_B T}} \quad (2.32)$$

Here, n_i is the intrinsic electron density, k_B the boltzman constant and T the temperature. Adding the current contributions (2.25), (2.26) and (2.30) together yields the total current of the diode:

$$J = J_n(-w_p) + J_p(w_n) + J_{SCR} \quad (2.33)$$

The full solution of this equation is beyond the scope of this report, but the solution will be described for the two most important scenarios; a solar cell in the dark and a solar cell under illumination. All the equations in this chapter can be found in Nelson's book [3] as well as the full solution to (2.33).

When a cell is connected to an external circuit and is not subjected to any radiation, it behaves like any other diode. A common model for the current is given by:

$$J_{dark} = J_0(e^{\frac{qV}{nk_B T}} - 1) \quad (2.34)$$

Here n is the ideality factor, q is the electron charge, V is the voltage over the diode, k_B is Boltzmann constant, T is the temperature in Kelvin and J_0 is the leakage current. It is normal to call the current that is present without illumination "dark current". n is an experimental parameter used to fit the theoretical curve to measured data. Under ideal conditions, when all recombination is in the neutral regions $n = 1$. If this is not the case n can be higher ($n \sim 2$). Effects of this will be studied further in subsection 2.4.

When a cell has an external electrical short circuit from the n-side to the p-side it is said to be under short circuit conditions. The short circuit allows current to flow and causes the voltage to be equal at both surfaces. When a cell is exposed to radiation it will produce a photocurrent, J_L . This photocurrent is a constant, for a given amount of illumination. In the depletion approximation the photocurrent and the dark current are linearly independent, and may be summed to give the total current:

$$J_{total} = J_{dark} + J_L \quad (2.35)$$

See fig. 2.7 for an illustration of how the short circuit current affects the dark current of a diode. This is a classic depiction of solar cell operation, and there are a few critical points on the graph. The points where J_{total} crosses the current- and voltage axis are called "Short Circuit Current" (I_{SC}) and "Open Circuit Voltage" V_{OC} , respectively. Short circuit current occurs is the maximum amount of current a cell can produce and occurs when the electrical poles of a cell are short circuited (ie. the load is zero). Open circuit voltage is the highest voltage a cell is able to produce, and occurs when there is no connection between the poles of a cell (ie. the load is infinite). The power a cell consumes or provides is the product of the current and voltage, through the equation:

$$P = UI \quad (2.36)$$

In the fourth quadrant where the current is negative but the voltage positive, the cell is supplying energy to the load. The points where this supplied power is highest is called the "maximum power point", and can be described by I_{mp} and V_{mp} in the fig. 2.7. A measure of the quality of a cell is given by the "Fill Factor":

$$FF = \frac{V_{mp}I_{mp}}{V_{OC}I_{SC}} \quad (2.37)$$

The efficiency of a solar cell is described by the following equation:

$$\eta = \frac{W_{out}}{W_{in}} \quad (2.38)$$

If a cell is subjected to uniform illumination the expression becomes:

$$\eta = \frac{V_{mp}I_{mp}}{I_{ill}A_{cell}} \quad (2.39)$$

Where I_{ill} is the intensity of the light and A_{cell} the area of the cell under investigation. Normally the light in this kind of experiment is calibrated to 100 mW/cm^2 . The current current-voltage characteristics of J_{total} in 2.7 is usually inverted (multiplied by -1) so the curve is in the first quadrant. This is done simply because it is easier to work with a curve in the first quadrant instead of the fourth.

2.3 Intermediate Band Solar Cells

Adding extra impurities to normal solar cell structures can under certain circumstances add additional energy levels to the material's band structure. This is normally considered a bad thing, as extra energy levels in the band gap increases Shockley-Read-Hall recombination. However, if the impurities are spread out evenly throughout the crystal and with a high enough density, the overlapping of quantum states can cause a new band of its own. Normally referred to as an "Intermediate band", charge carrier lifetimes can be high enough to allow charge carriers to clear the full band gap in two smaller energy jumps instead of one full. This allows light with lower energy than the full band gap to contribute to current generation.

Intermediate Band Solar Cells (IBSCs) are an emerging field and its methods are not yet fully determined. The most common choice for impurities are so called "quantum dots" (QDs). QDs are nanometer sized objects that provide an approximately zero dimensional potential well. As such, particles

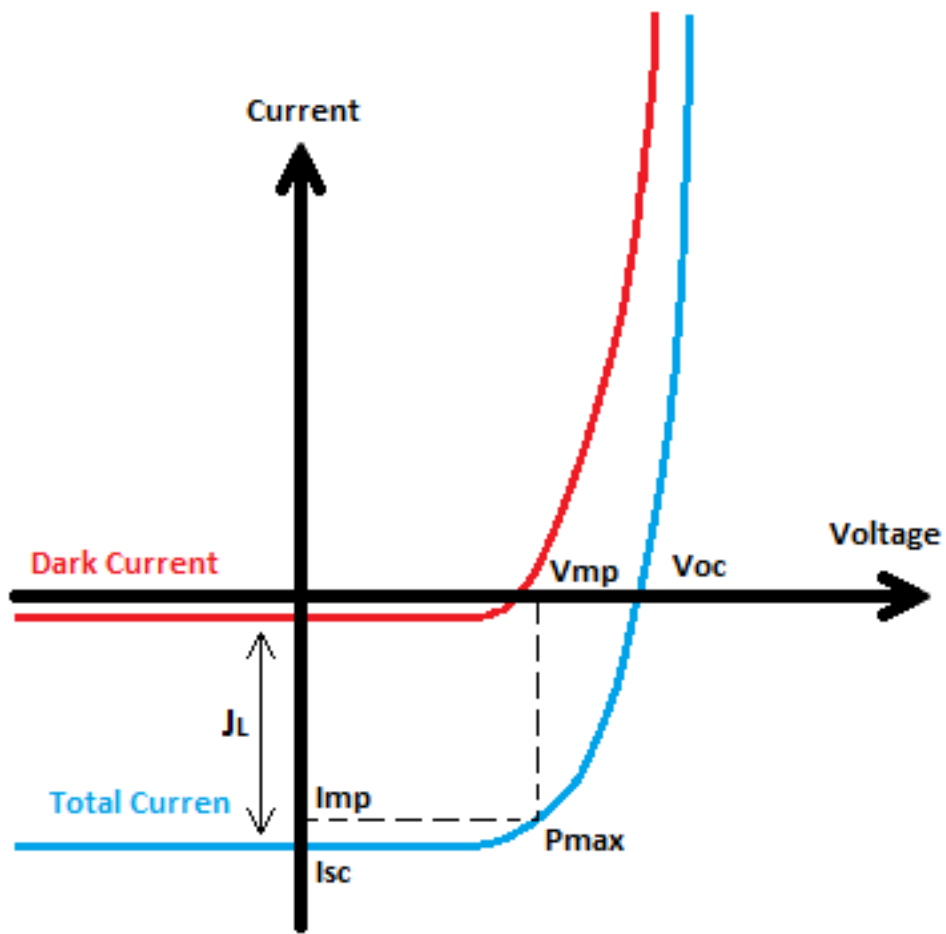


Figure 2.7: Graph showing the dark current of a diode, the offset caused by the light generated current and the total current of a diode under illumination.

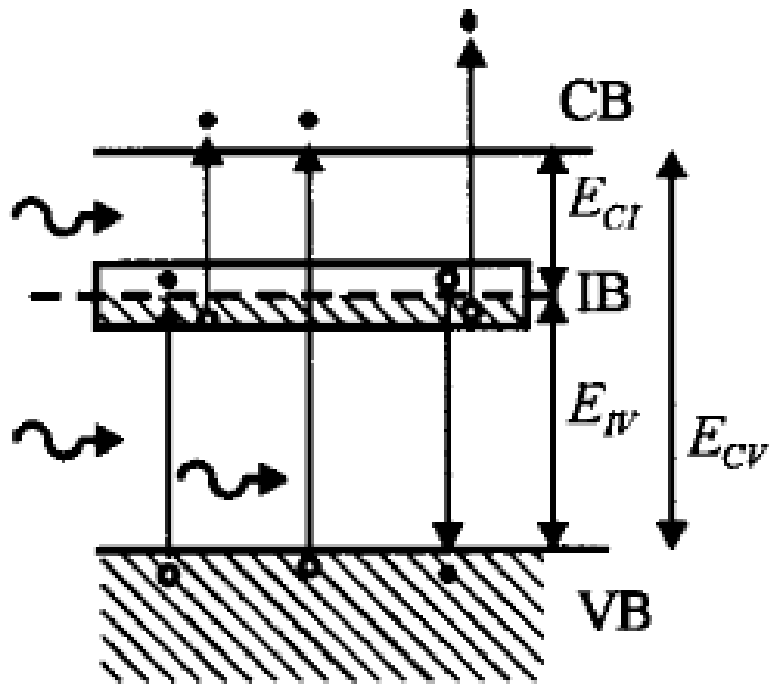


Figure 2.8: Illustration of the energy levels in an IBSC. Figure is taken from [5]

that occupy this potential well have no spatial degrees of freedom. Pauli-exclusion does not allow two identical particles to occupy the same state and as a result particles are forced to stack on top of each other (energetically). The details of these QDs are beyond the scope of this text, but it should be mentioned that stress effects of Indium-Arsenide (InAs) deposited on a Gallium-Arsenide (GaAs) substrate produces QDs. This is a common method of producing QD intermediate band solar cells, and the cells that have been analyzed in this thesis are of this design. Fig. 2.8 shows a qualitative image of a semiconductor with an additional, intermediate band. For further reading on QDIBSCs see [8].

2.4 Diode Models

The one- and two-diode models are simplifications of a solar cell where the complex characteristics of a real cell are broken down into basic circuit elements. The two-diode model contains an ideal current source, two ideal diodes and two ideal resistances. The ideal current source represents the generated current, J_L . The two diodes represent recombination currents. The two resistances account for series- and shunt resistances. Figures (2.9) and (2.10) show the circuit diagrams for the two models.

Examination of the two-diode circuit by means of simple circuit theory reveals that its output current can be written as

$$J = J_L - J_{01}\left(e^{\frac{V+JR_S}{n_1V_T}} - 1\right) - J_{02}\left(e^{\frac{V+JR_S}{n_2V_D}} - 1\right) - \frac{V + JR_S}{R_{SH}}. \quad (2.40)$$

Here J and V are the output current and voltages. J_L is the light-generated current. R_S and R_{SH} are the series and shunt resistances. Furthermore,

$$J_0\left(e^{\frac{V}{nV_T}} - 1\right) \quad (2.41)$$

is the standard expression for the current through a diode and is used twice in the expression above. Here J_0 is the saturation current, V the bias voltage, $V_T = k_B T/q$ is the thermal voltage and n the ideality factor. Solving equation 2.40 for J and V is not possible analytically, but numerical and iterative solutions are possible [9]. The diode models by themselves can give qualitative information about how different parameters affect the output of a solar cell. Fitting real-world measurements to the diode model can give quantitative information about the characteristics of the real cell. The diode models will be revisited in chapter 4.

2.4.1 The Interpretation of D_1 and D_2

When it comes to fitting equation 2.40 to measurements of real cells, there are some different schools of thought. With as many as eight adjustable parameters, it is easy to imagine the possibility of getting several equally good fits with different choices of parameters. J_L , R_S and R_{SH} affect the output current and voltage in a easily recognizable and predictable manner. See chapter 4. However, the two diodes complicates the matter. As we shall see D_1 and D_2 affect the *curvature* and V_{OC} of the current-voltage characteristics. In this thesis, the choice has been made to make the following assumptions:

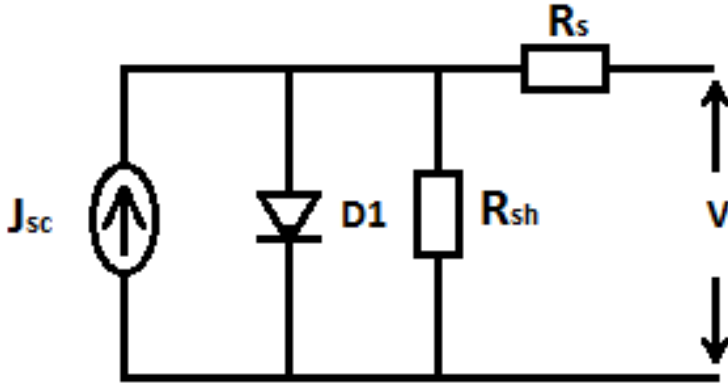


Figure 2.9: The one diode model.

$$n_1 = 1 \quad (2.42)$$

$$n_2 = 2 \quad (2.43)$$

Under these conditions one may view the contribution from D_1 to represent recombination currents in the neutral regions of the cell. D_2 can then be interpreted as the effect of recombination currents in the SCR. See for instance [10]. Other interpretations allow n_1 and n_2 to change. Setting $J_{02} = 0$ and allowing n_1 to vary produces a one-diode model with changing ideality factor. This method may also provide useful information, but is not considered here. Allowing all four diode parameters (n_1 , n_2 , J_{01} and J_{02}) to vary simultaneously may provide so many good fits that it is impossible to gather any useful information.

It should be mentioned that cells made from different materials are known for having different ideality factors. The ideality factors are also known to change as a function of bias voltage. This can be explained by the fact that the size of the SCR changes proportionally with the bias voltage. See fig. 2.11. This figure is taken from [6].

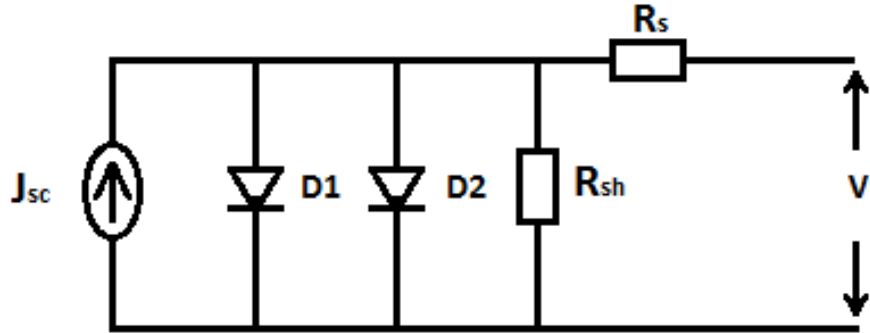


Figure 2.10: The two diode model.

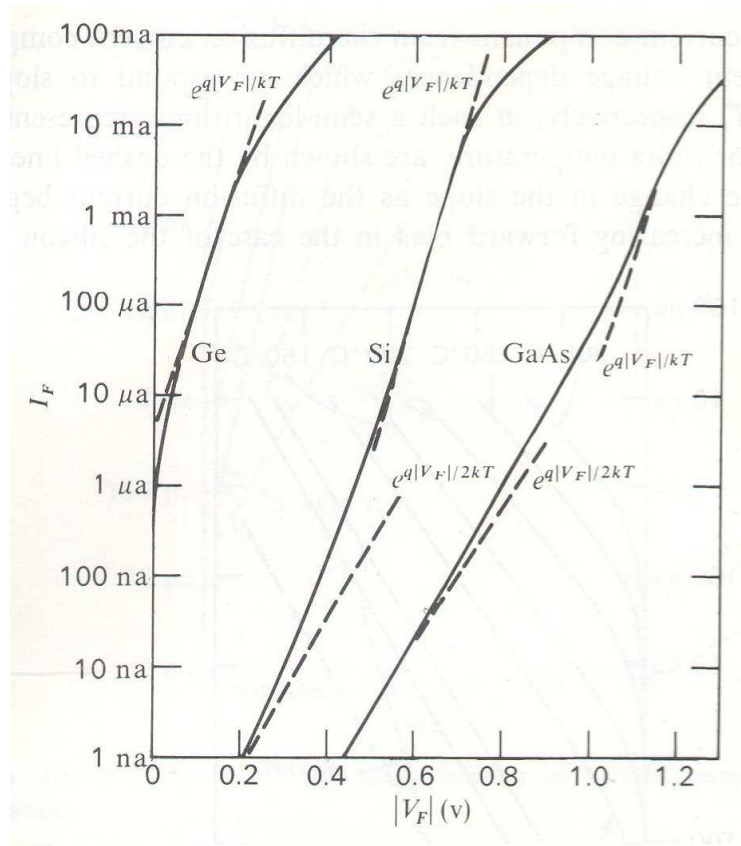


Figure 2.11: Different ideality factors for different materials and bias voltages.

Chapter 3

Continuation of Project Work

During the fall of 2010 the author of this paper was responsible for setting up the laboratory [4] used to provide some of the measurement data appearing in this text. This chapter consists of three parts. First comes an account of the changes that have been made since the fall of 2010. Second, in sub section 3.1, there is a user's manual for whomever will use the setup in the future. Lastly, a simple laboratory verification is undertaken in section 3.2. This is to show the capability and quality of the laboratory setup.

The setup is depicted in fig. 3.1. The lab can be found in room E4-118 in the Natural Sciences Building (Realfagbygget) at NTNU, but will be moved to an undecided location by fall 2011. Since the fall of 2010 a few changes have been made to the setup. As was described in the project work of 2010 [4], the laboratory equipment consist of the following: One lamp ("ABET Technologies Sun 2000 Solar Simulator") capable of producing an $AM1,5$ spectrum. A sourcemeter (Keithley 2440) capable of simultaneously measuring and sourcing currents and voltages with an uncertainty of $\pm 1\mu V$ and $\pm 0.1nA$. A PC with a *LabVIEW* virtual interface (VI) created by the author that controls the sourcemeter and provides a graphical interface for the laboratory user. It also stores measurement data at a location chosen by the user. A new addition to the setup is a metal box with a temperature regulator. This "thermobox" is situated under the lamp and the user is supposed to let the samples rest on it during measurements. If a good thermal connection is achieved, the box is able to keep the sample temperature at a level chosen by the user ($25^{\circ}C$ is the internationally accepted standard, and $22,5^{\circ}C$ is the lowest achievable temperature during steady-state operation). The lab has also been equipped with a reference solar cell and high-quality probes for measuring physically small contact points. Changes were made to the LabVIEW VI; the interface was restructured slightly and changed from Norwegian to English. A function testing whether or not the sourcemeter

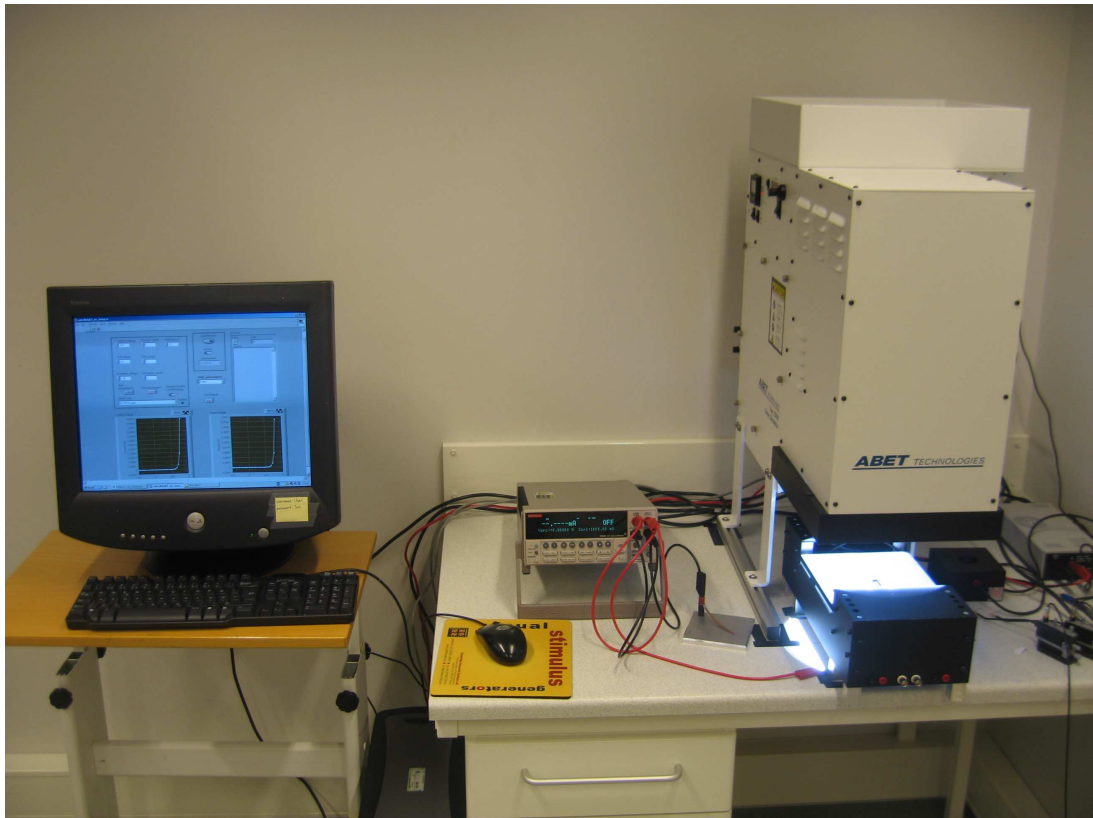


Figure 3.1: The laboratory setup.



Figure 3.2: The Solar Simulator Front Panel.

is switched on when the program is started was added. If the sourcemeter is off when the test is run, the function automatically stops the program from running. A new user was added to the computer with username "user" and password "Sol". A stand-alone version of the VI was created and a shortcut was placed on the desktop of "user". Originally, the thermobox was supposed to be controlled within and as a part of the VI. However, this was abandoned and a decision was made to use its original regulator instead of a "home made" one. A shortcut to this regulator is also placed on the desktop of "user". The original regulator allows for far larger control of how the thermo-box is regulated (P/PI/PID and choices of constants, etc.) and has been found to work nicely.

3.1 Instructions of Use

3.1.1 The Solar Simulator

The following is a description of how to use the equipment mentioned above to get current-voltage characteristics of sample solar cells. Firstly the Solar Simulator needs to be switched on. The lamp requires about 15 minutes to heat up before it supplies a good *AM1.5* spectrum. It is powered on by flicking an on/off switch at its back, around the right hand side. Flicking this switch starts the lamp's cooling fan and embedded computer systems. Fig. 3.2 shows the solar simulators front panel. All things on the front panel are not of equal importance for taking simple IV measurements. Switch nr. 1 and knob nr. 4 controls the arc-bulb that provides the light for the experiments. Normally switch 1 is in the 'off' position. Holding it down to the 'preset' position shows the previous 'lamp current' setting on the display. Turning knob 4 changes the preset lamp current. When switch 1 is switched to the 'on' position, the arc-bulb is ignited. There is a shutter in front of the lamp opening that is able to block the light from the lamp. This is meant to allow the user to dim the light between measurements without switching it off. The Shutter Control (2) should be set to 'Internal', as this allows the user to control the shutter by switch 3. Switching 3 between 'open' and 'close' opens and closes the shutter. With the current setup at the time of writing ~ 21.3 A gives an illumination of 100 mW/cm^2 .

The lab is equipped with reference solar cell may be used to tune the illumination level to 100 mW/cm^2 . The cell is from 'Rera Systems' and has been shunted. Measuring the voltage over the shunt allows with a voltmeter/sourcemeater allows for a determination of the illumination. The cell has been found to apply a voltage of 87.3 mV over the shunt under AM 1.5 conditions. A user can use either the sourcemeater or a voltmeter to measure this voltage. Certified wires are as well as a calibration letter is kept with the cell in the lab. See fig. 3.3 for an illustration.

To avoid damage to the arc-bulb upon shut-down, the simulator should never be switched completely off directly after measurements. Switch of the arc-bulb first by switch 1 and leave the lamp cooling system running for at least 15 minutes before powering down the Simulator completely.

3.1.2 Sourcemeater and Computer

The sourcemeater can be operated alone as a stand alone unit, and the reader is referred to its user manual to see how this is done (All manuals regarding equipment in the lab can be found in the cupboard at the far side of the

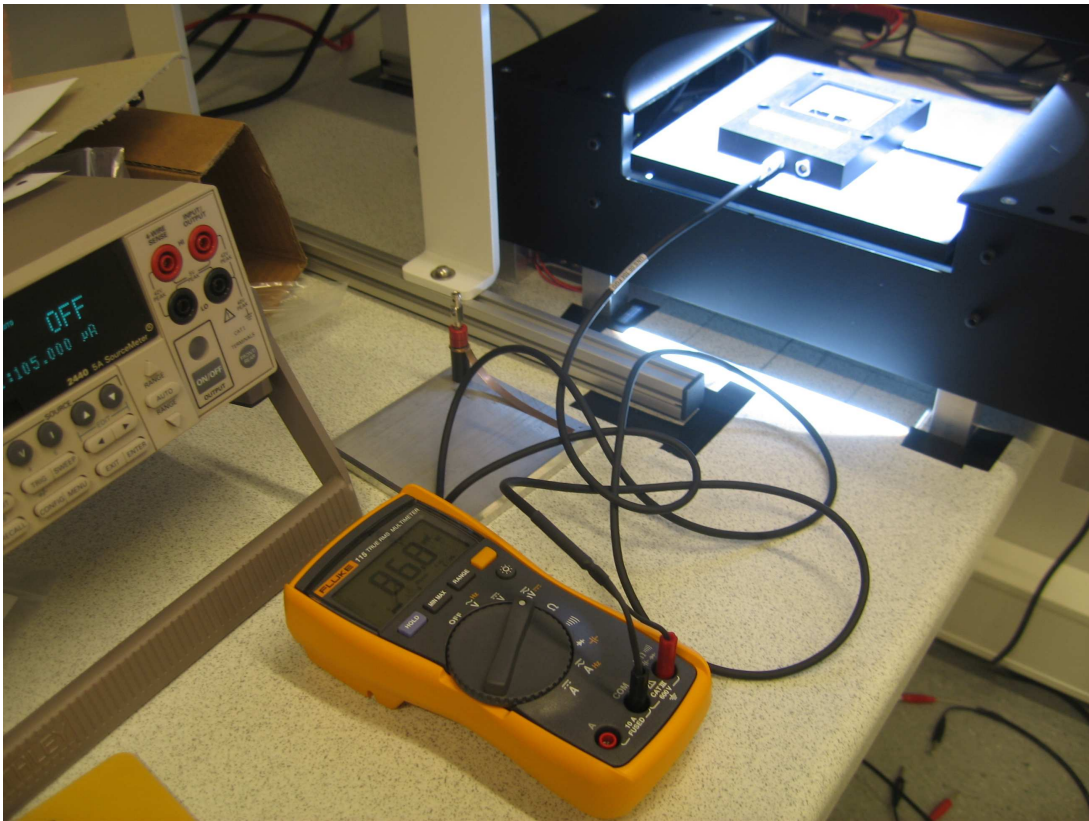


Figure 3.3: Calibration of the Solar Simulator.



Figure 3.4: Sourcemeter Front.

room). It is turned on with the on/off button on the front. There are four electrical connections at the front, two red and two black. See fig. 3.4. The two red connections are over the black connections and the colors represent their electrical polarity (red is positive, black is negative). During measurements the two red connections should be connected electrically to the p-side of the sample solar cell. The two black connections should be connected to the n-side.

After switching on the computer and logging on to "user" with the password "Sol", a shortcut to "Solar VI" can be found on the desktop. When the program is opened the user sees the front panel. The front panel consists of one main measurement block, one smaller block for quick measurements, VISA address-input, error output, two graphs and a QUIT button. See fig. 3.5.

The main measurement block is used to take proper measurements of a cell's IV characteristics. There are nine boxes where the user can input information regarding the experiment. The user inputs for the main measurement block are; Starting voltage, End voltage, Increment voltage, starting current, End current, Increment current, Dwell-time and Sample note. In addition there is a sliding knob called "Variable to be swept". The sliding knob allows the user to choose what quantity should be measured as a function of the other. If it is set to "voltage", the program will measure the current as a function of a sourced voltage and vice versa. The starting, ending and increment current and voltage inputs program the sourcemeter to start sourcing either a current or a voltage (depending on the position of the current/voltage knob) at the starting value. It will then increase the chosen variable by the

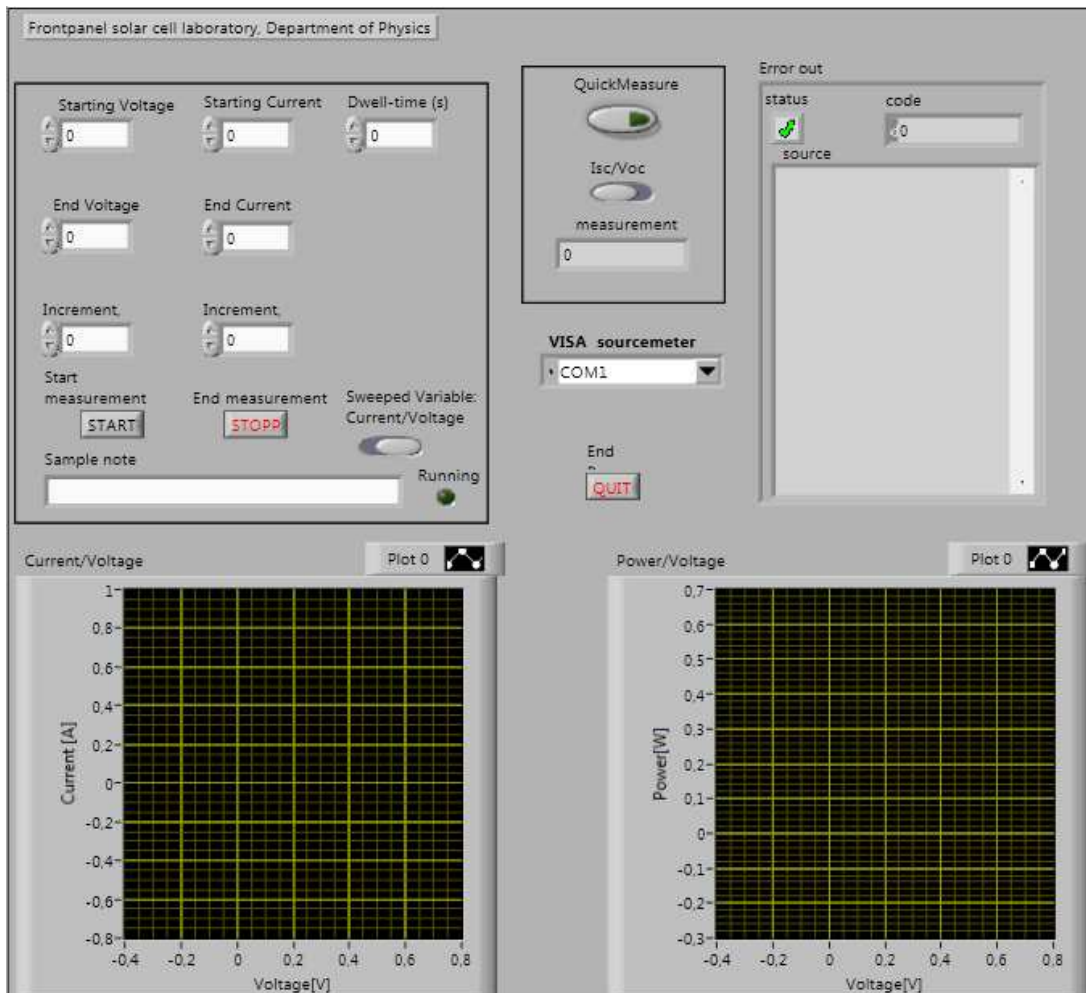


Figure 3.5: Frontpanel of LabVIEW VI.

increment until it reaches the end value. If the start value is chosen to be higher than the end value and the increment is negative, the sourcemeter will go from high to low output. The dwell time causes the sourcemeter to wait a certain amount of seconds between each successive measurement. This allows the user to compensate for slow settling times in the sample. The box labeled sample note takes in a string and prints it in the output file. In addition to these user inputs there is a START button, STOP button and a "LED" to show when the setup is doing measurements. The two graphs show the results from the measurement. One graph plots the IV-curve and the other plots the power output as a function of the voltage. After each measurement the program will prompt the user for a directory to save the file to. The data is saved as text-files. See appendix B for an example.

Next to the main measurement block is a smaller one with only three elements. This is the quick-measure block. It allows the user to quickly determine the open-circuit voltage and short-circuit current. When the green button is pressed, the sourcemeter will measure V_{OC} or I_{SC} depending on what alternative is chosen on the knob. It is advised to use this method when determining the V_{OC} and I_{SC} of a sample. The result is posted in the number box. Pressing the large QUIT button terminates the program.

3.1.3 The Thermo-Box

The user manual for the thermobox can be found printed out at the lab together with the other manuals, as well as electronically on the desktop of the lab computer. A shortcut to the original control program is placed on the desktop of 'user'. When opened a user should click 'open file', then 'PVlab'. This opens a ready made configuration created by the author. After opening the configuration the user should choose 'connect' then 'send'. The thermo box is then programmed to stay around 25 °C and is regulated with a PI regulator with the values $P = 60$ and $I = 2$. This has been found to work nicely for the purpose of the lab.

3.2 Verification of Laboratory Setup

To check the quality of the laboratory setup, two sets of measurements were taken of a new batch of NTNU-made quantum-dot intermediate band solar cells. The two measurement sets were made about a month apart, the first one on the 16th of May and second on the 18th of June of 2011. Although the cells are grown in Trondheim (NTNU), they had been sent to Madrid (Spain) for processing. The team in Madrid (IBLAB at Instituto de Energi

Solar, Universidad Politecnica de Madrid) have also measured the current-voltage characteristics of the cells, and these measurements are have been used as a reference. The results of the comparisons are shown in the graphs 3.6, 3.7, 3.8 and 3.9. As a test of the reproducibility of the measurements, the results of the 16/5 and 18/6 measurements where divided by each other to give their ratio. The results can be seen in fig. 3.10. The curves marked as 'Our measurements 16/5' are the measurements done on the 16th of May, while the curves marked 'Our measurements 18/6' the ones made on the 18th of June. The results marked with 'Spain' are the results found by the Spanish group. Table 3.1 shows critical data points for all three data series of all cells analyzed in the verification.

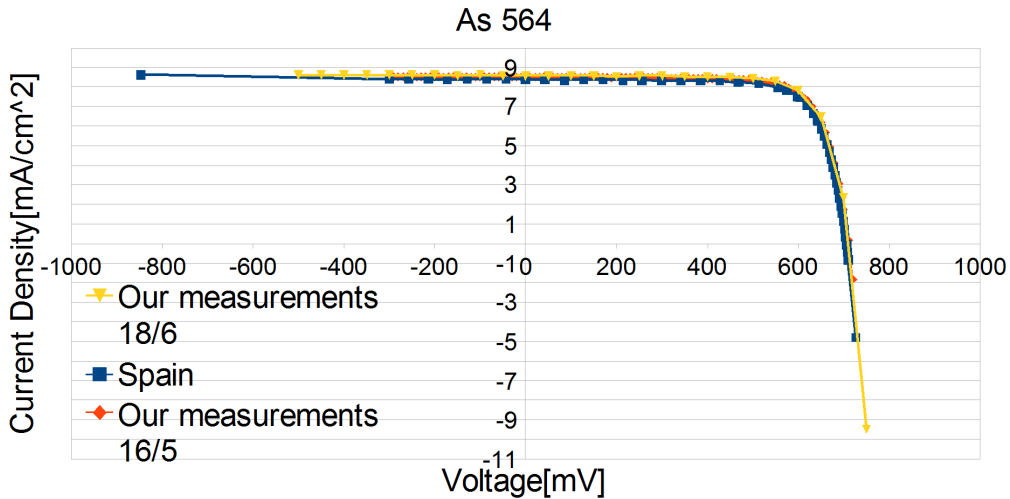


Figure 3.6: Different measurements made on cell As 564.

As one can see from the figures, the laboratory setup seems to give credible and stable results. In fig. 3.10 one can observe a deviation from unity towards the right hand side of all the curves. However, this is most likely caused by the V_{OC} of the cells occurring in these regions. As both current measurements are approaching zero at V_{OC} , dividing one on the other is likely to produce unreliable and diverging results. If one ignores the results close to the V_{OC} of the cells one can see that a certainty of $\pm 2\%$ may be assumed on the basis of this analysis.

It should be mentioned that the our setup subjects the samples to an illumination of 100 mW/cm^2 . The Spanish group have done their measurements at an illumination of 90 mW/cm^2 , to conform with the latest industry standards. To make the different setups comparable all our current density values have been multiplied by a factor 0.90.

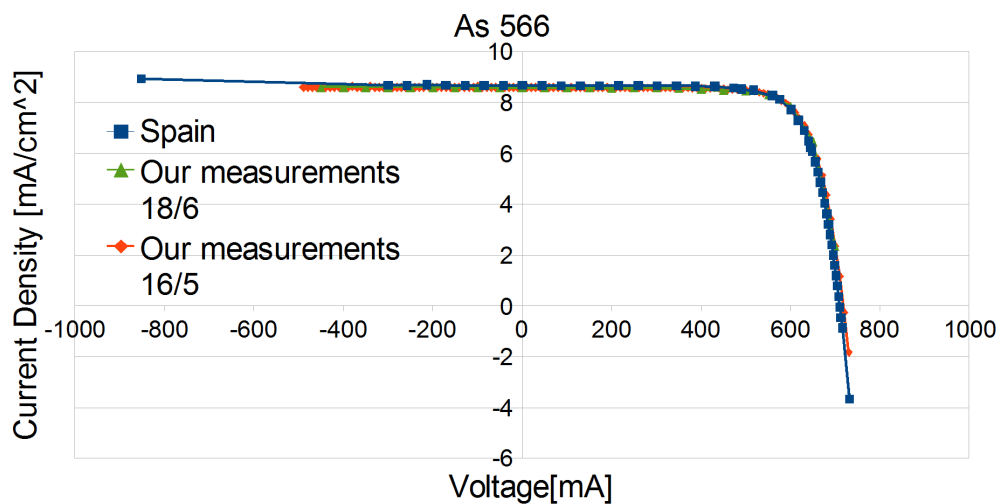


Figure 3.7: Different measurements made on cell As 566.

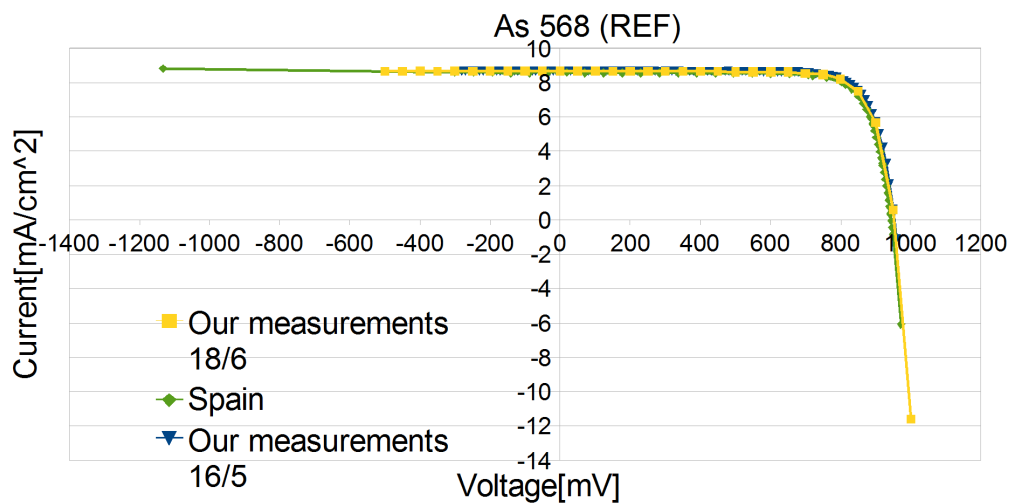


Figure 3.8: Different measurements made on cell As 568.

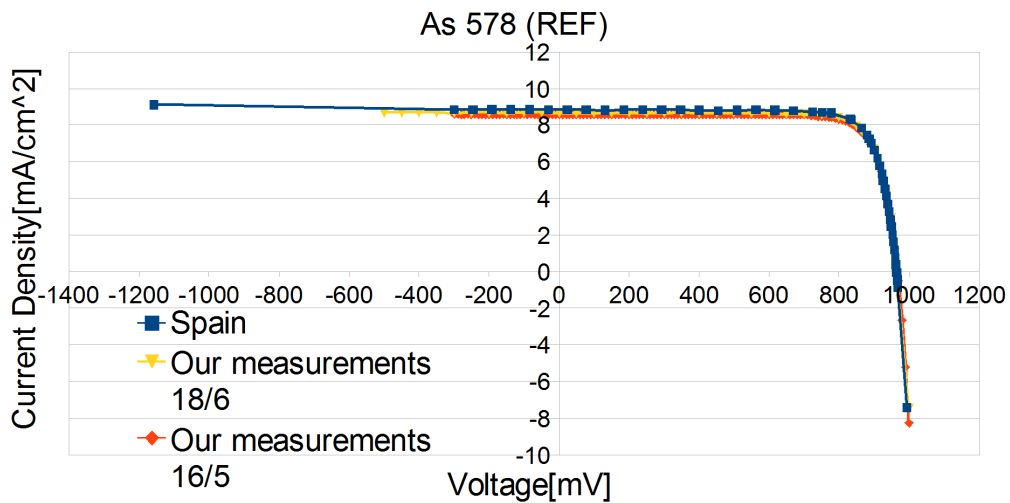


Figure 3.9: Different measurements made on cell As 578.

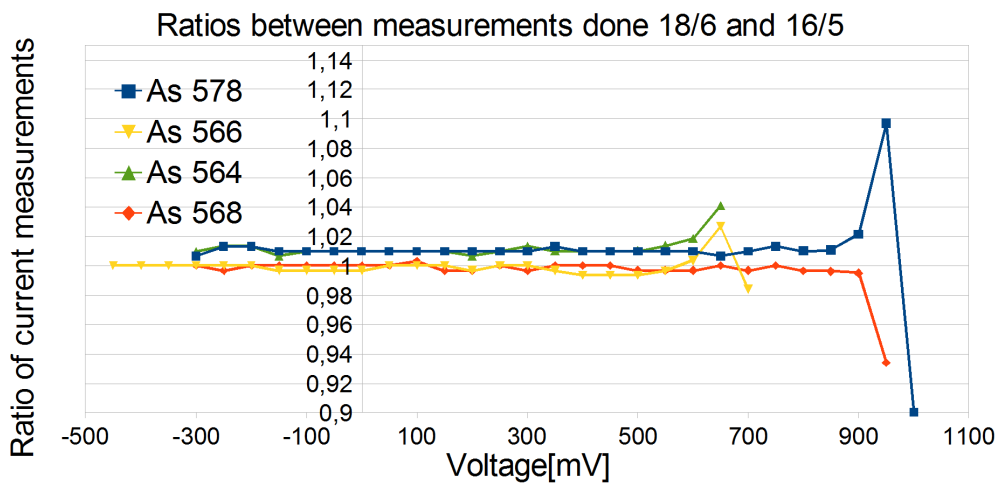


Figure 3.10: Current measurements made on 18/6 divided by current measurements made on 16/5. Plotted against the voltage at which the measurements were taken.

Table 3.1: Measured Cell data

Cell Name	$V_{OC}[V]$	$I_{SC}[A]$	$J_{SC}[mA/cm^2]$
As 564, 16/5-'11	0.712605	0.000300	8.49
As 564, 18/6-'11	0.715773	0.000302832	8.57
As 564, Spain	0.706	-	8.38
As 566, 16/5-'11	0.714258	0.000300	8.49
As 566, 18/6-'11	0.717955	0.000303733	8.60
As 566, Spain	0.71	-	8.68
As 568(REF), 16/5-'11	0.950522	0.000301	8.519
As 568(REF), 18/6-'11	0.952417	0.000305171	8.637
As 568(REF), Spain	0.944	-	8.58
As 578(REF), 16/5-'11	0.966448	0.000302	8.547
As 578(REF), 18/6-'11	0.968803	0.000305639	8.65
As 578(REF), Spain	0.964	-	8.83

Chapter 4

Simulations

It was decided that a fair amount of time should be spent experimenting with two-diode model simulations. The purpose of this was firstly to get acquainted with the behavior of the two-diode model and secondly to attempt a comparison between simulated and measured data. After some discussion it was found that the simplest solution was to use the free *OrCAD Demo v 16.3* available from www.cadence.com. This is a bundle package that among other things include *pSpice Schematics*. These programs work together to provide a simple electric circuits simulator that allows the user to add/remove parts, change parameters and simulate parameter sweeps. The simulated data can then be exported as a text file. Copying the data into a spreadsheet program, such as *Microsoft Excel* or *Libre Office Spreadsheet*, allows for further data analysis. It has been found to work, but can be time consuming. The simulations were carried out by constructing the circuit in fig. 4.1. Executing a parameter sweep on the value of R_LOAD from almost zero ($\sim 0,01$ m Ω) to almost infinite (~ 100 k Ω) allowed extraction of the current voltage characteristics. Measuring the voltage across and current through the load during the sweep gave the simulated output of the 'solar cell'.

4.1 The parameters of the two-diode model

The two-diode model has eight degrees of freedom: Current (J), series resistance (R_s), shunt resistance (R_{sh}), ideality factors of the two diodes (n_1) and (n_2), the saturation currents of the two diodes (j_{01}) and (j_{02}) and the simulated ambient temperature (T). Their typical values can be seen in table 4.1. It should be noted that setting (j_{01}) or (j_{02}) to zero produces the one-diode model with ($n = 1$) and ($n = 2$), respectively.

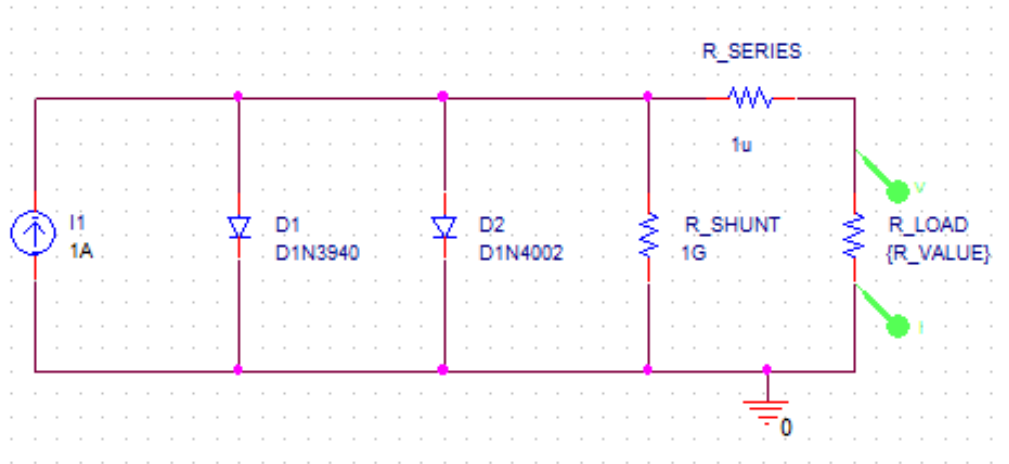


Figure 4.1: The two-diode model in OrCAD/pSpice.

Table 4.1: Two-diode model parameters.

Parameter	Typical value
J	~ 1 A
R_s	~ 1 Ω
R_{sh}	~ 10 k Ω
n_1	~ 1
n_2	~ 2
j_{01}	$\sim 10^{-15}$
j_{02}	$\sim 10^{-8}$
T	~ 300 K

4.1.1 The Ideal Case

The natural startingpoint for an analysis of the diode models is the ideal one-diode with $J = 1$, $R_s = 0$, $R_{sh} = \infty$, $n_1 = 1$, $j_{01} = 10^{-14}$ and $T = 300$ K. See figure 4.2. This choice of parameters gives a perfect IV-curve and a maximum fill factor, 86% in this case. It is a good example of the output of an ideal solar cell.

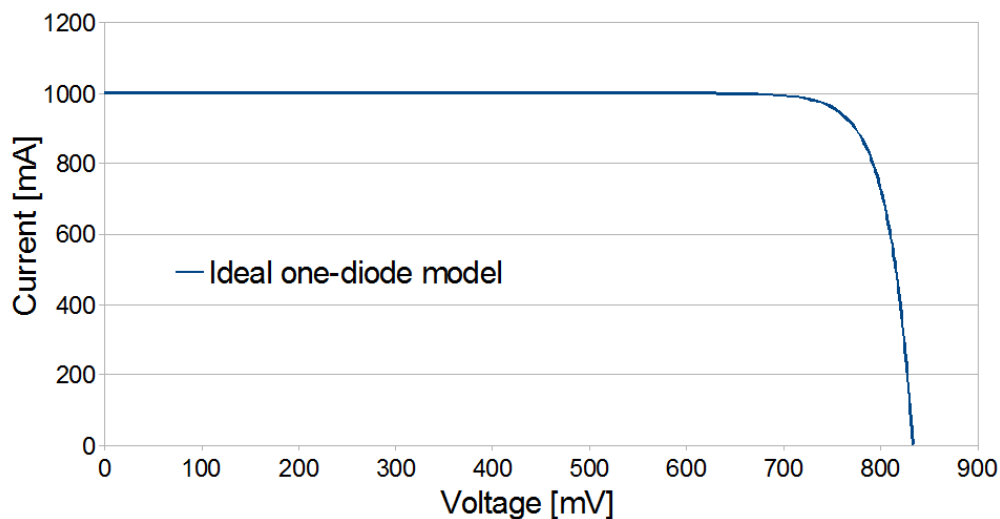


Figure 4.2: The output of the ideal one-diode model.

4.1.2 Parasitic Resistances

Parasitic resistances are unavoidable in physical solar cells and can degrade the cell's output. The effect of an increasing series resistance can be seen in fig. 4.3. As can be seen in the simulations, the series resistance does not change the V_{OC} , but affects the I_{SC} if it is large enough. Series resistance is caused by all resistive effects from the contacting at the base and emitter of the cell and further out through to the load. A series resistance decreases the fill factor.

A shunt resistance is caused by a short circuit allowing charge carriers to flow from the base of a cell to the emitter without passing through an external circuit. A shunt resistance should ideally be as high as possible. It does not affect I_{SC} but degrades the fill factor and can decrease V_{OC} . See fig. 4.4.

Fig. 4.5 shows the effect of both a high series- and a low shunt resistance. The ideal case is also shown. The unideal case has $R_s = 0.1$ and $R_{sh} = 5$. It

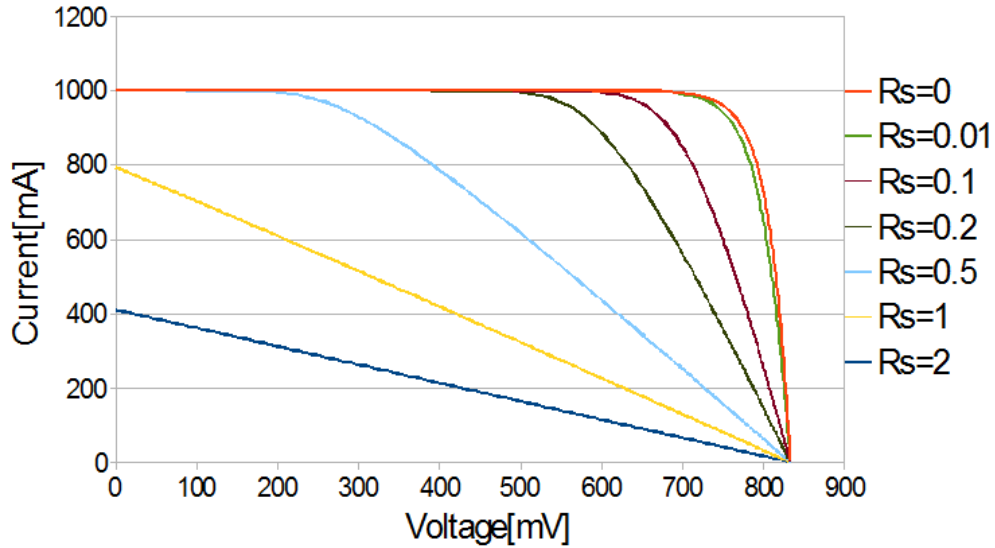


Figure 4.3: Output of the two-diode model with changing series resistance.

should be noted that both I_{SC} and V_{OC} is decreased slightly in this case.

If both a high series- and low shunt resistance is present, the IV-characteristics may look like fig. (4.5).

4.1.3 Increased Current

It is normal to assume that the amount of current from the diode model current source is linear with the illumination of the physical cell. As such, changing the amplitude of the current simulates a changing physical illumination. As can be seen from fig. (4.6) an increased illumination increases the overall current linearly. It can be seen that V_{OC} also is increased, but by a much smaller factor.

4.1.4 Temperature Effects

The IV-characteristics is affected by the ambient temperature. The linear temperature-dependence of the saturation currents (j_{01} and j_{02}) causes the V_{OC} to decrease with increased temperature, as can be seen in fig. 4.7. It is also known that the I_{SC} increases slightly with temperature [7], however this does not show up in the two-diode simulations done in this thesis. This is the only point throughout this work where the two-diode model fails to give realistic results, and should therefore be subject to great caution. One

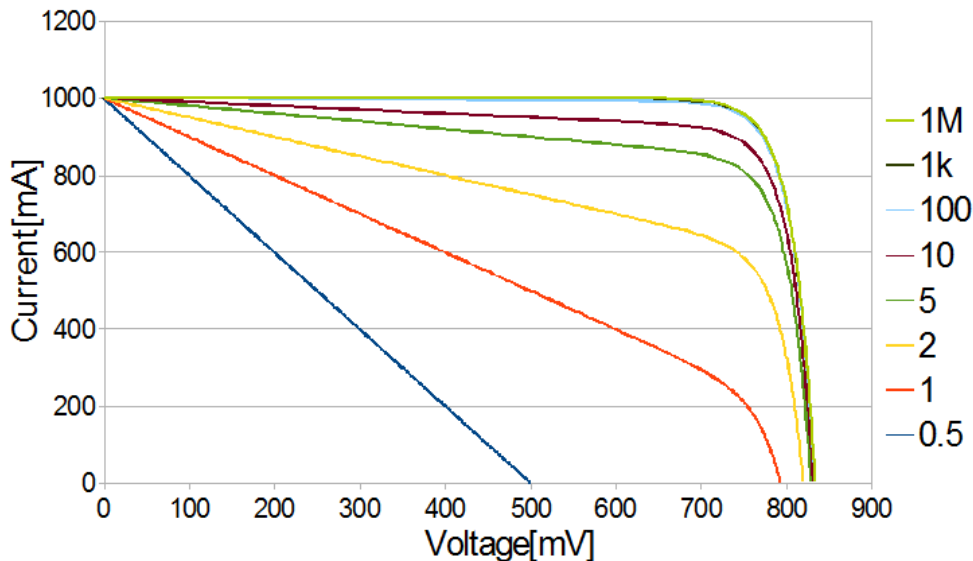


Figure 4.4: Output of the two-diode model with a varying shunt resistance.

might be able to include a temperature dependent current source in the diode models that could account for this issue.

4.1.5 Ideality factors

The ideality factors of the two diodes, D_1 and D_2 , are usually left unchanged in the two-diode model. Their role in the IV-output is similar to the saturation currents, namely to determine at what voltage the diode in question begins conducting and the curvature of the IV-characteristics. As can be seen in equation (2.40) the flow of current through any one diode is inversely proportionate to its ideality factor and proportionate to its saturation current. Setting $n_1 = 1$ and $n_2 = 2$ allows the diode currents to be interpreted as recombination currents in the neutral- and space charge regions, respectively. To illustrate the role of the ideality factor, its effect on the *one-diode* model can be seen in fig. 4.8. The saturation is kept constant at $j_{01} = 10^{-14}$.

4.1.6 The Saturation Currents

Arguably the most interesting aspect of the two-diode model, the saturation currents of diodes D_1 and D_2 affect V_{OC} and curvature of the IV-characteristics. If the ideality factors are kept constant, $n_1 = 1$ and $n_2 = 2$, changing J_{01} and J_{02} is the only way of manipulating the curvature. As real current-voltage characteristics almost never have curvatures similar to the

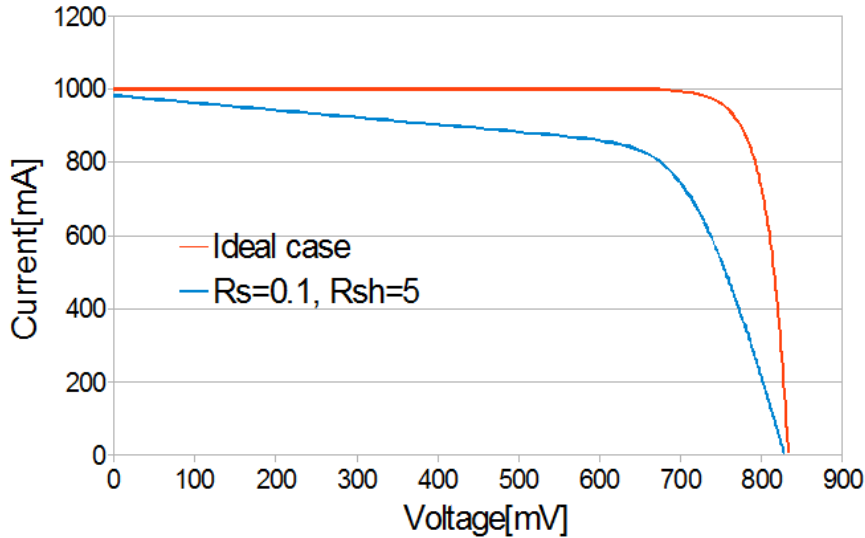


Figure 4.5: The effect of both a high series- and a low shunt resistance on the IV-curve.

one-diode mode with $n_1 = 1$, the necessity of the two-diode model is apparent. To achieve a realistic IV-curve, one must almost always include both diodes. In other words: Realistic characteristics always contain contributions from both diodes.

Fig. 4.9 illustrates the difference between the one-diode and two-diode models. The graph shows four IV-characteristics with equal I_{SC} and V_{OC} , but with different curvature around the point of maximum power (V_{MP} and I_{MP}). These results are not possible to achieve in the one-diode model without changing the ideality factor. Changing the saturation currents J_{01} and J_{02} shifts the focus from one diode to another. This can be interpreted as shifting the focus from one ideality factor to another. This changes both the curvature and pushes the V_{OC} higher. If one wishes to keep the V_{OC} at the same point, as it is in 4.9, one needs to *decrease* the saturation current of the opposite diode. This only works up to a certain degree, after which the current flowing through the opposite diode is so small that it can be ignored, and one is left with the one-diode result. The graph of fig. 4.9 contains two one-diode results. The first is the classical IV-curve with $n = 1$ and $J_0 = 10^{-14}$. It can be recognized as the curve with the highest fill factor. The second one-diode curve has $n = 2$ and $J_0 = 10^{-7}$. It can be recognized as the curve with the lowest fill factor. The two curves with fill factors between these two extrema are two-diode models with contributions from both the $n = 1$ and $n = 2$ diodes. As can also be seen, the ratio between them is changed. If one

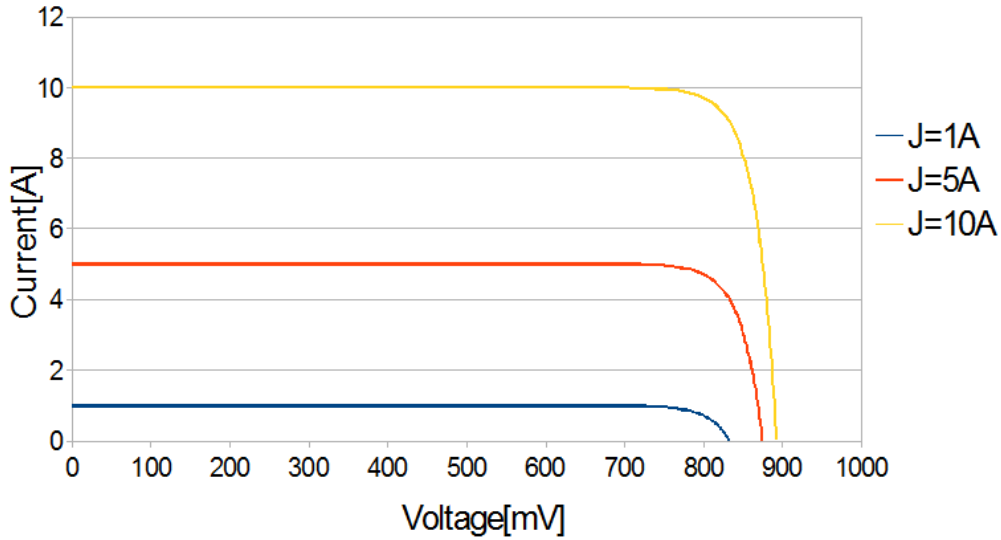


Figure 4.6: Two-diode model output with increasing current

imagines the ratio between the two saturation current to be a 'weight' that decides how heavily each of the two ideality factors are represented in the curve, one can see that all the curves between the $n = 1$ and $n = 2$ one-diode results can be produced by shifting this 'weight'. Hopefully, this weight can provide information regarding where and to what degree recombination is occurring in a cell.

As can be seen in table 4.1 the value of j_{02} is generally around 10 million times larger than j_{01} . Because D_2 conducts as $j_{02}e^{qV/2k_bT}$, it must have such a large value before it starts to compare to D_1 . Setting $j_{01} = j_{02}$ produces the same results as the one-diode model with $n = 1$. In other words, One might as well set $j_{02} = 0$. Fig. 4.10 shows how the two-diode output changes with j_{02} . It shows IV-characteristics for the two-diode model with the value of j_{02} changed linearly from low to high. It starts of at the same value as j_{01} and is increased by a factor of 10 until it is unity.

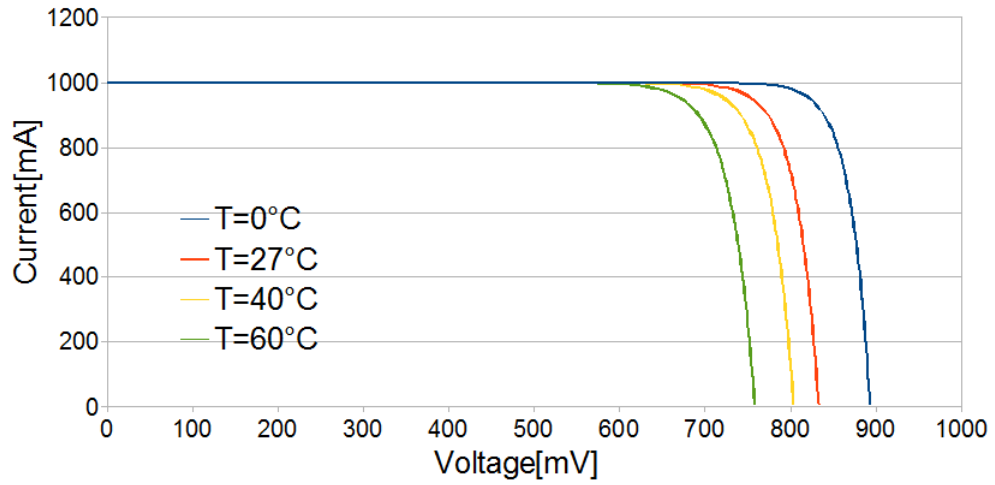


Figure 4.7: The effect of temperature on the two-diode model output. Notice that the current is not affected as it would have been in a physical cell.

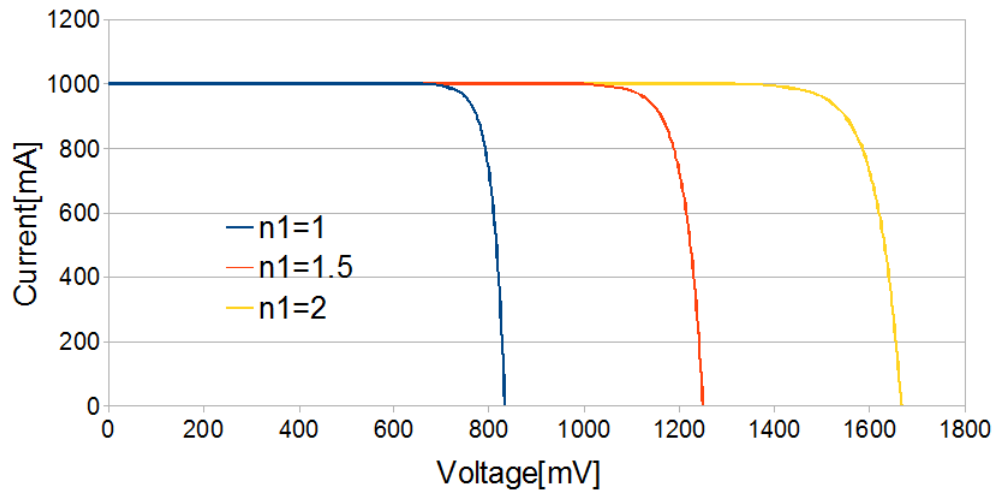


Figure 4.8: The effect of n_1 on the one-diode model. $j_{01} = 10^{-14}$.

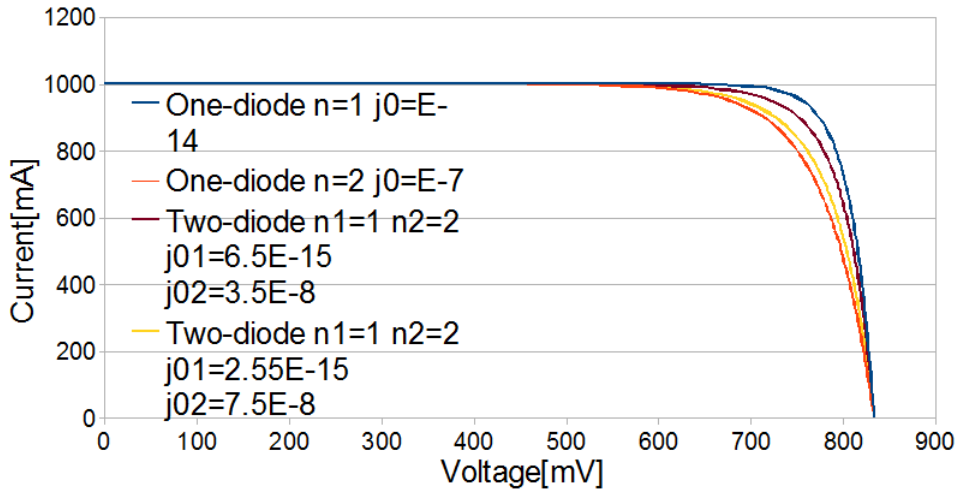


Figure 4.9: The gained degree of freedom by the addition of a second diode to the one-diode model.

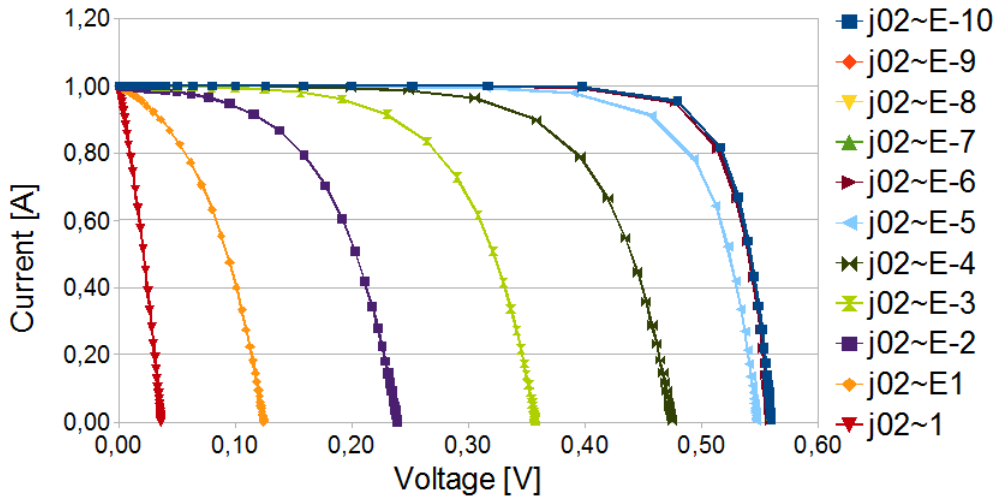


Figure 4.10: The effect of j_{02} on the two-diode model.

Chapter 5

Results

The cells investigated in this thesis are InAs/GaAs quantum dot intermediate band solar cells grown in cooperation between the Dept. of Physics and the Dept. of Electronics and Telecommunications at NTNU. All the cells were sent to Spain for processing. Afterwards the best eight cells were sent back for further examination. The cells are presented in table 5.1. The cells were examined as described in chapter 3.

5.1 Measurements

The results of the measurements are presented in table 5.2 and a typical result is shown in fig. 5.1. Current-voltage characteristics for all cells are shown in appendix A. Fig. 5.2 shows the results for all the cells together. All measurements were taken at an illumination of 100 mW/cm^2 and *AM1.5* spectrum. The temperature was $25 \text{ }^\circ\text{C}$.

5.2 Curve Fitting

Many attempts were made at curve fitting IV-characteristics from the one- and two-diode model to measured data. This was done by the same means as discussed in chapter 4 with OrCAD/pSpice. This has proven to be extremely difficult and time consuming. The only worthwhile result is presented in fig. 5.3.

Table 5.1: QDIBSCs

Name	Growth T	In:As ratio	QD layers	Additional information
As 564	470°C	1:9	5	QDs grown in cycles GaAs Ref cell, no QDs, w. accidental quantum well QDs grown continuously GaAs Ref cell, no QDs
As 566	520°C	1:9	5	
As 567	520°C	1:9	5	
As 568	520°C	-	-	
As 569	520°C	1:9	5	
As 570	520°C	1:37	5	
As 578	520°C	-	-	
As 579	470°C	1:9	20	

Table 5.2: Results

Name	V_{OC} [mV]	J_{SC} [mA/cm ²]	FF [%]	efficiency [%]
As 564	715	9.4	76	5.1
As 566	717	9.6	76	5.2
As 567	801	9.2	79	5.9
As 568	952	9.6	80	7.3
As 569	736	9.3	76	5.2
As 570	703	9.1	78	5.0
As 578	968	9.5	81	7.5
As 579	721	7.6	75	4.2

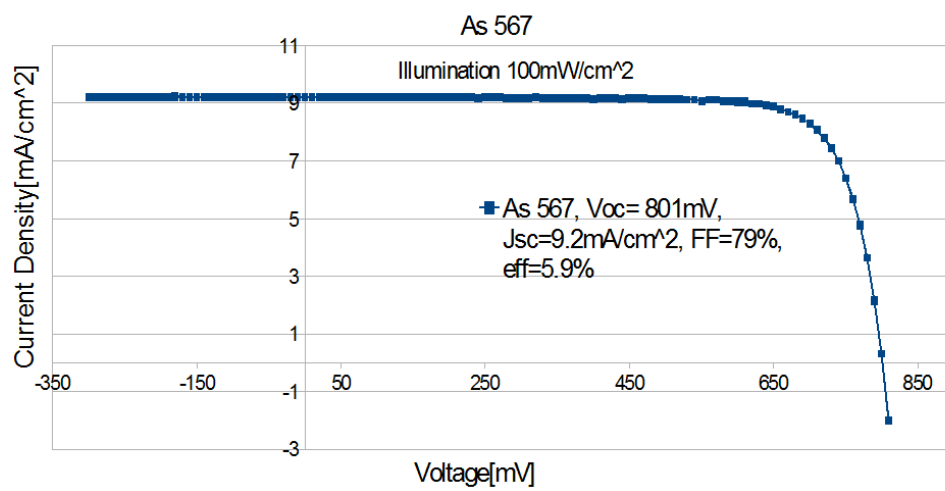


Figure 5.1: IV-characteristics for cell As 567.

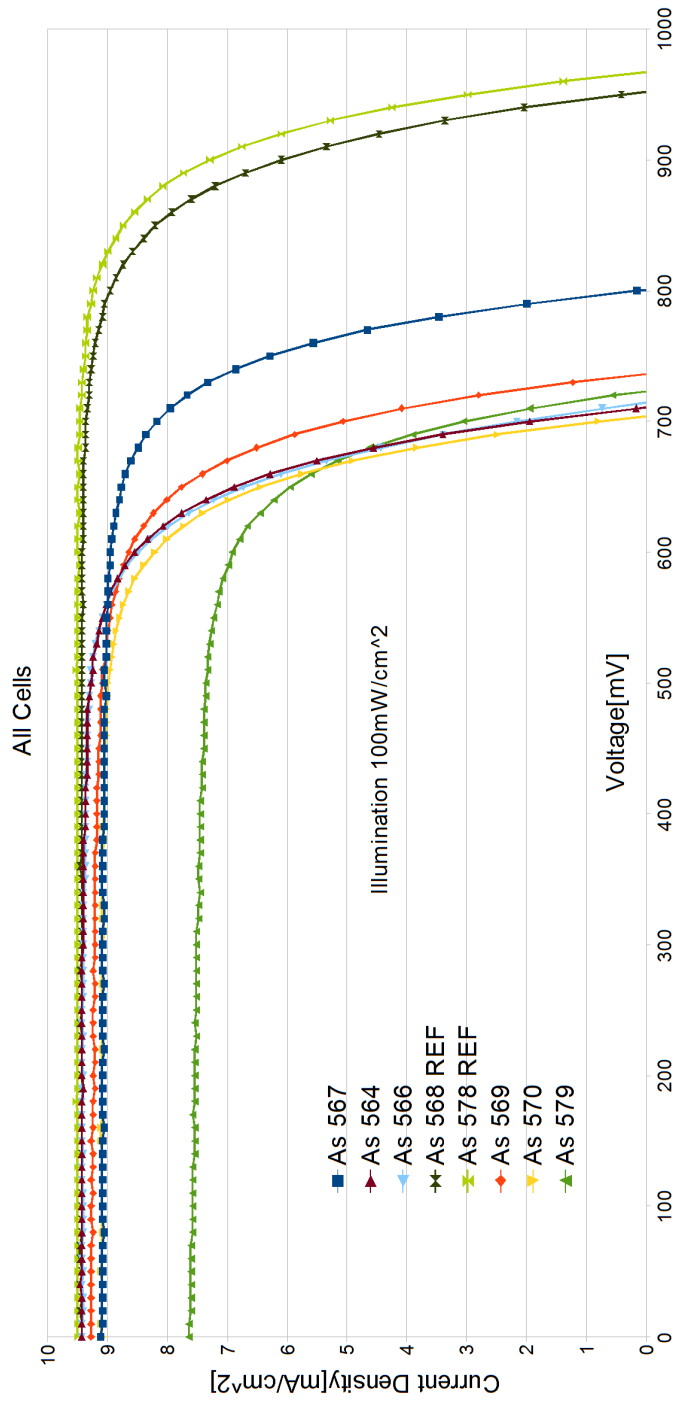


Figure 5.2: Current-voltage characteristics of all cells.

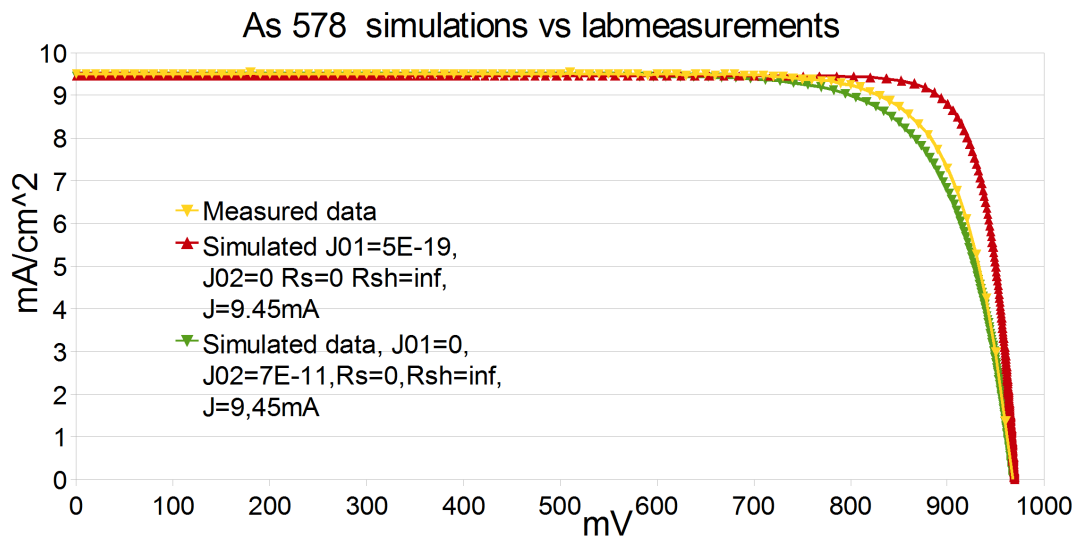


Figure 5.3: An attempt at curve fitting.

Chapter 6

Discussion

Although it may not seem like much, there is quite a bit to be learned from the results. Firstly, manual curve fitting is almost always a waste of time and should not be the basis of any scientific work. This, however, was not the goal of this thesis. The investigatory part of this thesis was made to examine the one- and two-diode models and their potential for analyzing solar cell performance. It seems the two-diode model is able to reproduce all the possible characteristics of a real cell; the only problem is being able to efficiently uncover the parameters.

An inspection of fig. 5.3 reveals a few things. This graph shows three curves, two simulated and one measured from cell 'As 578'. The two simulated curves show the two extrema of the two-diode model, namely the one-diode model with $n = 1$ and $n = 2$, respectively. As can be seen from the figure, the characteristics of the real cell seem to be somewhere in the middle of the two extrema, slightly closer to the one with $n = 2$. Since the cell in question is a pure GaAs cell, and the bias voltage range is between 0 V and 1 V, the result that the diode ideality factor seems close to $n = 2$ agrees with fig. 2.11. At this point the graph should be compared to fig. 4.9. As one may see these two graphs look very similar, apart from the fact that they have different V_{OC} , but this can easily be changed for the simulated case. Fig 4.9 is also a graph showing the two extrema of the two-diode model. In addition there are two curves between them showing the effect of a varying ratio of contribution from both diodes. It is easy to imagine the curve of 'As 578' in fig 5.3 being a two-diode model curve with a combined contribution from both diodes. If one had been able to reproduce the exact ratio of the two so that the simulated data would fit exactly with the measured data, one might be able to draw a conclusion as to where in the cell (physically) the dominating recombination is occurring. It is this information that is one of the big possibilities with two-diode model analysis.

However, as already mentioned, curve fitting should be done automatically by means of a specially written computer program. See for example [9]. If such a program were written, and it should not prove too hard to do, two-diode parameter analysis could be used as a strong tool in IV-characterization of solar cells.

Chapter 7

Conclusions and Further Work

Firstly, the solar cell characterization equipment set up during the fall of 2010 has been improved and tested. The improvements are the addition of a temperature regulator, small alterations to the software, improved user interface and the addition of electrical probes and a reference cell. Its quality and the reproducibility of its data have been examined, and it has been found to have a precision of at least $\pm 2\%$. The temperature regulator works well, and allows the lab user to control the temperature of the samples during measurements.

Secondly, the current-voltage characteristics and efficiencies of eight NTNU-made QDIBSCs have been examined. The results of this examination can be seen in table 5.2 and in appendix A.

Thirdly, a study of the two-diode model has been undertaken and its potential for use in solar cell analysis has been examined. It has been found to hold potential, but that a specially written curve fitting computer program is required before it can be used for any serious analysis. If such a program is acquired or written, it is highly probable that the fitting of two-diode model parameters to real cell data can provide useful information in the future.

Therefore, the writing or purchase of such a program is highly recommended and considered a natural next step for further work in this field.

Bibliography

- [1] Willson, Mordvinov, *Geophys. Res. Lett.*. Secular total solar irradiance trend during solar cycles 2123, 30(5), 1199, 2003.
- [2] Green, Emery, Hishikawa, Warta, *Prog. Photovolt: Res. Appl.***19**:84-92. Solar cell efficiency tables (v. 37) Wiley InterScience, 2011.
- [3] Nelson, *The Physics of Solar Cells*. Imperial College Press, London, 2003.
- [4] Vilpponen *Photovoltaic Characterization Laboratory*. Project work, NTNU, 2010.
- [5] Luque et al. *Journal of Applied Physics* **96**, 903-909, ,General equivalent circuit for intermediate band devices: Potentials, currents and electroluminescence, 2004.
- [6] Grove, *Physics and Technology of Semiconductor Devices*, p. 190, ,John Wiley & sons, Inc., 1967.
- [7] Vernon, Anderson *Applied Physics Letters* **26**, 707-709, Temperature effects in Schottky-barrier silicon solar cells, 1975.
- [8] Luque, Marti, *Advanced Materials* (**22**) 160-174, ,The Intermediate Band Solar Cell: Progress Toward the Realization of an Attractive Concept, 2010.
- [9] Hovinen, *Physica Scripta* (**T54**) 175-176, ,Fitting of the Solar Cell IV-curve to the Two Diode Model, 1994.
- [10] Manning, Gow, *IEE Proc.-Electr. Power Appl.* **146**, 193-200 ,Development of a photovoltaic array model for use in power-electronics simulation studies, 1999.

Appendix A

Current-Voltage characteristics for all cells

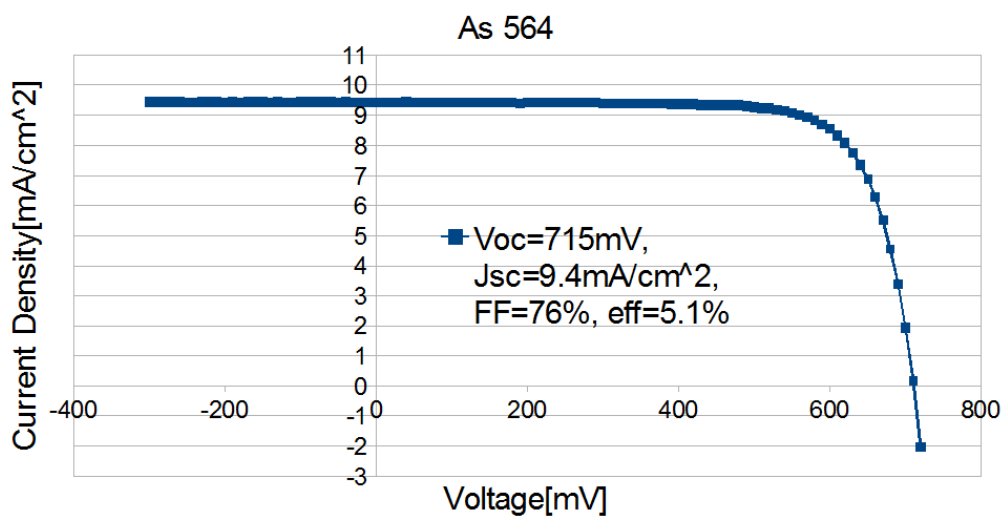


Figure A.1: Current-voltage characteristics for cell no. As 564.

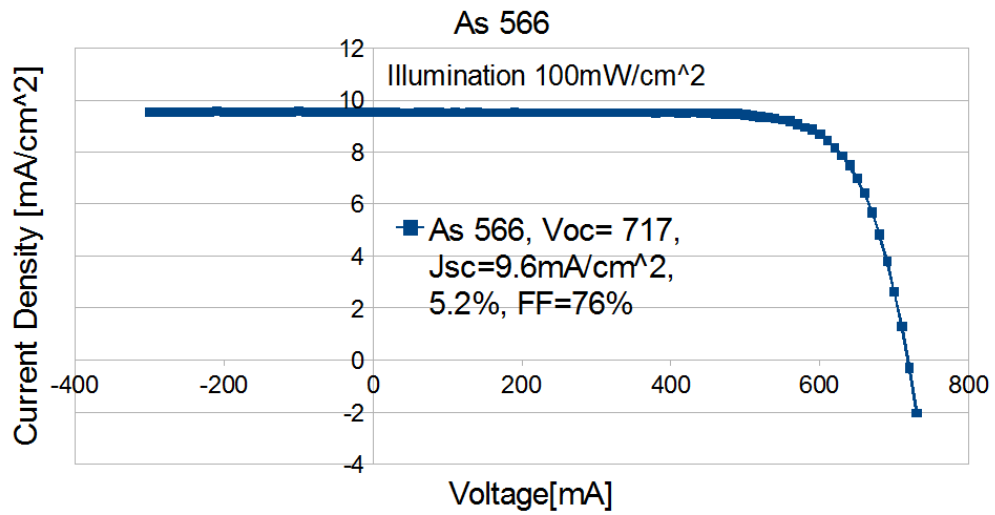


Figure A.2: Current-voltage characteristics for cell no. As 566.

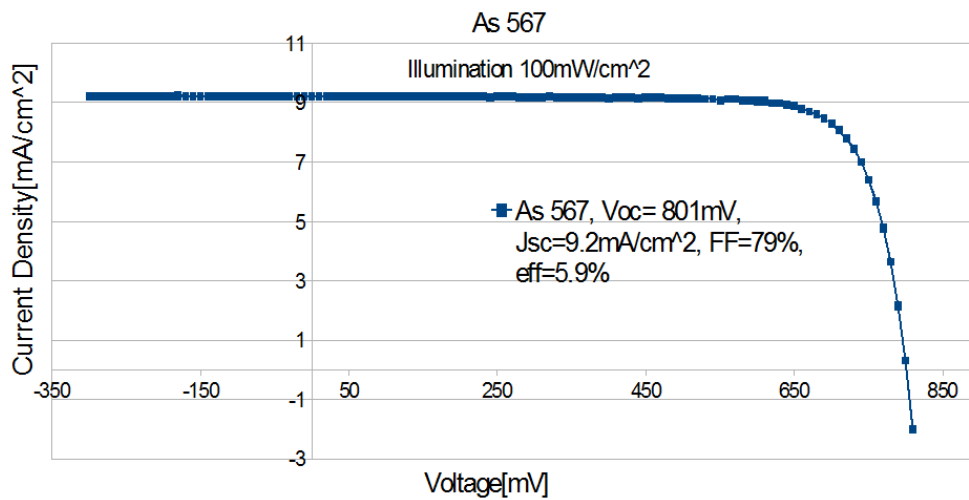


Figure A.3: Current-voltage characteristics for cell no. As 567

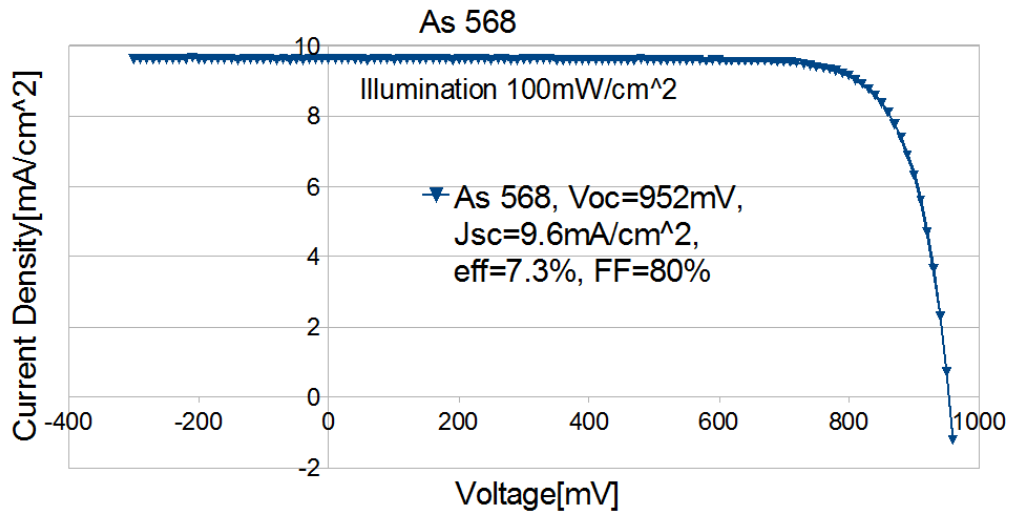


Figure A.4: Current-voltage characteristics for cell no. As 568

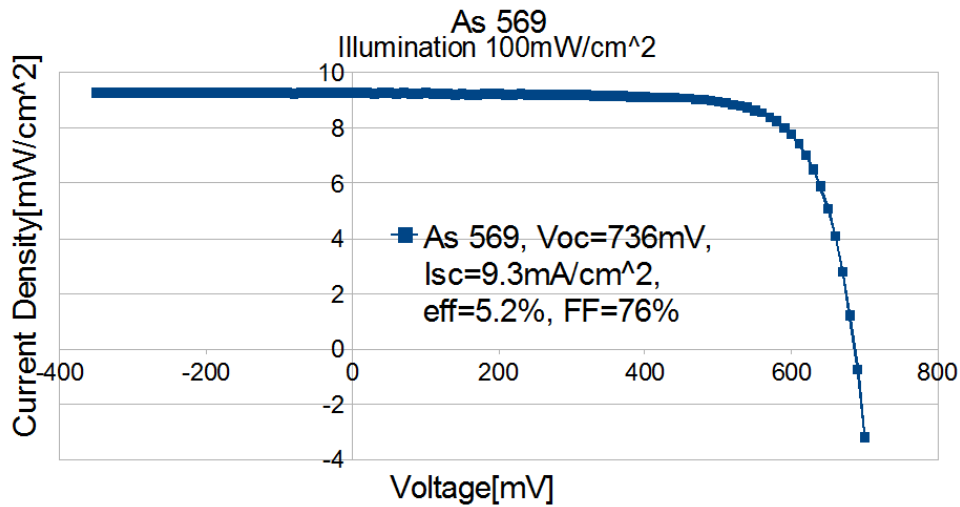


Figure A.5: Current-voltage characteristics for cell no. As 569.

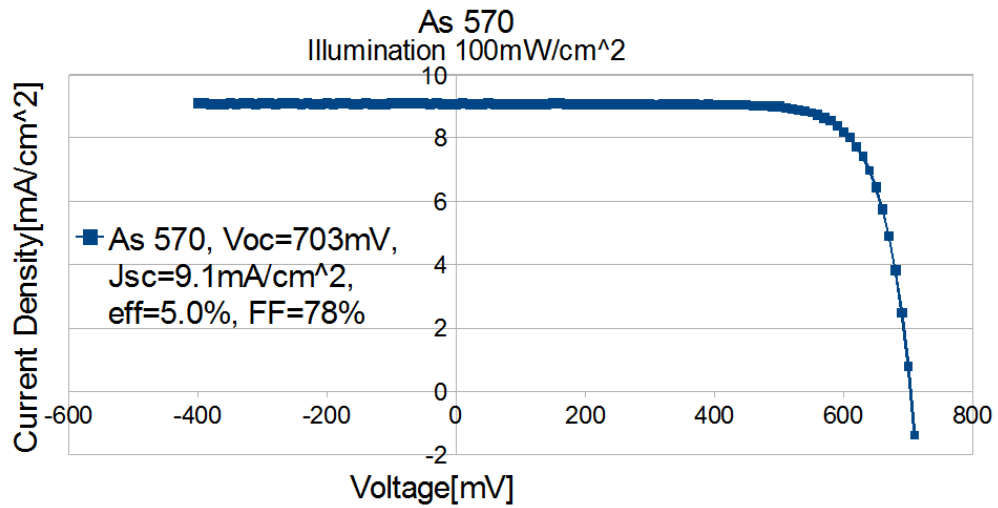


Figure A.6: Current-voltage characteristics for cell no. As 570.

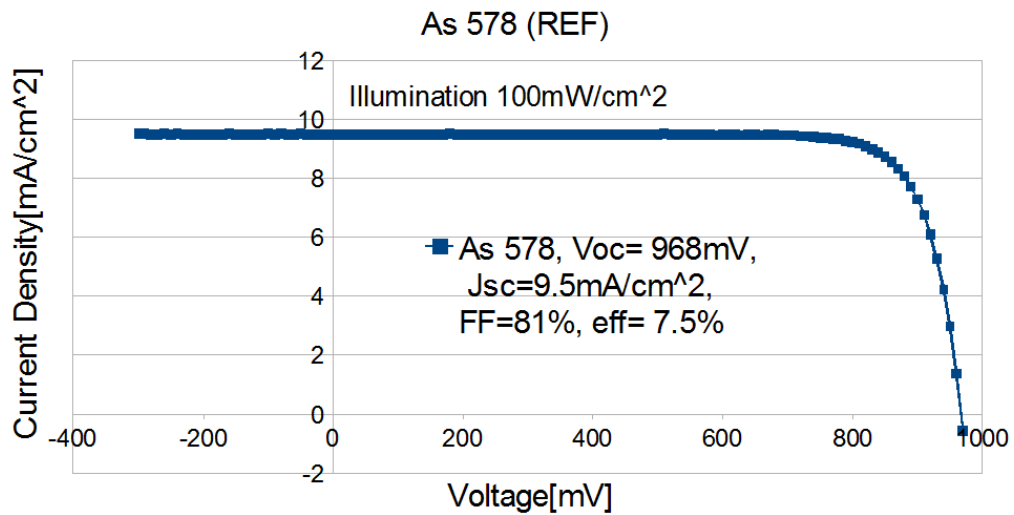


Figure A.7: Current-voltage characteristics for cell no. As 578

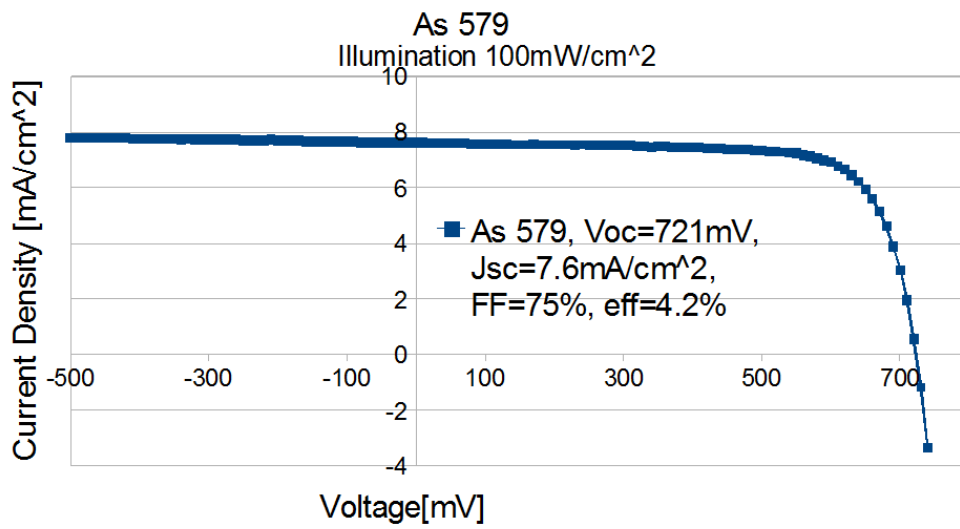


Figure A.8: Current-voltage characteristics for cell no. As 579.

Appendix B

Output file

```
LabVIEW Measurement
Writer_Version 2
Reader_Version 2
Separator Tab
Decimal_Separator .
Multi_Headings Yes
X_Columns Multi
Time_Pref Relative
Operator User
Date 1904/01/01
Time 01:00:00
***End_of_Header***
```

```
Channels 3
Samples 62 62 1
Date 2011/05/16 2011/05/16 2011/05/16
Time 15:44:42.046875 15:44:42.046875 15:44:42.046875
X_Dimension Time Time Time
X0 0.0000000000000000E+0 0.0000000000000000E+0 0.0000000000000000E+0
Delta_X 1.000000 1.000000 1.000000
***End_of_Header***
```

```
X_Value Untitled X_Value Untitled 1 X_Value Untitled 2 Comment
0.000000 -1.957680 0.000000 -0.000305 SPAIN CELL As 578, Dwell Time (milliseconds):500
1.000000 0.787092 1.000000 -0.000295
2.000000 0.830740 2.000000 -0.000285
3.000000 0.853634 3.000000 -0.000275
4.000000 0.869058 4.000000 -0.000265
5.000000 0.880260 5.000000 -0.000255
```

6.000000 0.889573 6.000000 -0.000245
7.000000 0.896882 7.000000 -0.000235
8.000000 0.903428 8.000000 -0.000225
9.000000 0.909465 9.000000 -0.000215
10.000000 0.914289 10.000000 -0.000205
11.000000 0.918988 11.000000 -0.000195
12.000000 0.922727 12.000000 -0.000185
13.000000 0.926732 13.000000 -0.000175
14.000000 0.930364 14.000000 -0.000165
15.000000 0.933541 15.000000 -0.000155
16.000000 0.936524 16.000000 -0.000145
17.000000 0.939475 17.000000 -0.000135
18.000000 0.941990 18.000000 -0.000125
19.000000 0.944535 19.000000 -0.000115
20.000000 0.946914 20.000000 -0.000105
21.000000 0.949294 21.000000 -9.500000E-5
22.000000 0.951424 22.000000 -8.500000E-5
23.000000 0.953409 23.000000 -7.500000E-5
24.000000 0.955492 24.000000 -6.500000E-5
25.000000 0.957376 25.000000 -5.500000E-5
26.000000 0.959152 26.000000 -4.500000E-5
27.000000 0.960969 27.000000 -3.500000E-5
28.000000 0.962640 28.000000 -2.500000E-5
29.000000 0.964266 29.000000 -1.500000E-5
30.000000 0.965983 30.000000 -5.000000E-6
31.000000 0.967448 31.000000 5.000000E-6
32.000000 0.968990 32.000000 1.500000E-5
33.000000 0.970379 33.000000 2.500000E-5
34.000000 0.971808 34.000000 3.500000E-5
35.000000 0.973158 35.000000 4.500000E-5
36.000000 0.974473 36.000000 5.500000E-5
37.000000 0.975770 37.000000 6.500000E-5
38.000000 0.977115 38.000000 7.500000E-5
39.000000 0.978301 39.000000 8.500000E-5
40.000000 0.979592 40.000000 9.500000E-5
41.000000 0.980738 41.000000 0.000105
42.000000 0.981936 42.000000 0.000115
43.000000 0.983067 43.000000 0.000125
44.000000 0.984192 44.000000 0.000135
45.000000 0.985265 45.000000 0.000145
46.000000 0.986362 46.000000 0.000155

47.000000	0.987345	47.000000	0.000165
48.000000	0.988397	48.000000	0.000175
49.000000	0.989451	49.000000	0.000185
50.000000	0.990446	50.000000	0.000195
51.000000	0.991437	51.000000	0.000205
52.000000	0.992434	52.000000	0.000215
53.000000	0.993385	53.000000	0.000225
54.000000	0.994337	54.000000	0.000235
55.000000	0.995256	55.000000	0.000245
56.000000	0.996135	56.000000	0.000255
57.000000	0.997060	57.000000	0.000265
58.000000	0.997947	58.000000	0.000275
59.000000	0.998823	59.000000	0.000285
60.000000	0.999665	60.000000	0.000295
61.000000	1.000529	61.000000	0.000305